Prepared for

NATIONAL AERONAUTICS AND SPACE ADMINISTRATION
Headquarters
Washington, D. C. 20546

Dr. F. F. Marmo, Project Director and
Principal Investigator

January 1969

EXPERIMENTAL AND THEORETICAL STUDIES IN PLANETARY AERONOMY

Quarterly Progress Report

Covering the Period 1 September 1968
Through 30 November 1968

Prepared under Contract No. NASW-1726

TABLE OF CONTENTS

I. INTRODUCTION

This second Quarterly Progress Report described the technical progress achieved from 1 September 1968 through 30 November 1968 under NASA Contract No. NASw-1726. Scientific investigations accomplished during the reporting period resulted in the generation of the following papers submitted and/or published in accredited scientific journals, or presented at scientific meetings.

Technical Papers Submitted and/or Accepted for Publication

a. Submitted:

Formation of N_4^+ in Nitrogen (P. Warneck)	J. Geo. Res.
Dipole Properties of Molecular Hydrogen (G. A. Victor and A. Dalgarno)	J. Chem. Phys.
Higher Ionization Potentials of Nitric Oxide (J. A. R. Samson)	Phys. Letters

b. Published:

Primary Processes in the Photolysis of SO_2 at 1849Å (P. Warneck, et al)	J. Chem. Phys., 72, 3736 (1968)

Technical Papers Presented at Scientific or Professional Meetings

Higher Ionization Potentials of Molecules Determined by Photoelectron Spectroscopy (J. A. R. Samson) - 21st Annual Gaseous Electronics Conference, University of Boulder, Boulder, Colorado, 16-18 October 1968.

In Section II, technical summaries are presented on the work performed during the current reporting period. Section III contains brief summaries of technical papers presented at scientific and/or professional meetings as well as other miscellaneous topics of interest in the performance of the current contract committments. Finally, in compliance with the requirements of the contract, an integrated tabulation by labor category and grade of total hours expended in the execution of the contract, for the specified reporting time interval, is included in Section IV.

II. SUMMARY OF TECHNICAL WORK PERFORMED FOR THE PERIOD 1 SEPTEMBER 1968 THROUGH 30 NOVEMBER 1968

The technical progress accomplished during the current reporting period can be conveniently described in terms of the two major categories contained in the statement of work: (A) laboratory studies, and (B) theoretical studies.

A. LABORATORY STUDIES

In accordance with the subject work statement, it is required to perform the following laboratory investigations on selected planetary atmospheric gases: (1) measure drift velocities and ionic mobilities, (2) acquire quantitative VUV photon scattering cross section data with emphasis on the spectral regions displaying discrete and/or continuous ionization and/or absorption features, (3) measure the kinetic energies of photoelectrons generated by EUV photoionization, (4) measure the absorption and photoionization cross sections for $\lambda\lambda < 500\text{Å}$, (5) acquire VUV ($\lambda\lambda$ 1050Å - 2000Å) high resolution absorption cross section data with emphasis on the minor constituents of planetary atmospheres, (6) measure rates of ion-neutral reactions, and (7) measure the yield and kinetic energy of photoionization fragment ions.

During the current quarterly reporting period, the bulk of the laboratory effort has been directed toward accomplishing task items (1), (2), (3) and (4) above. Brief descriptions of the progress achieved is given below in the order indicated.

1. Drift Velocity Measurements for Atmospheric Ions

In the course of investigating drift velocities of N_2^+ ions formed by photoionization of nitrogen, it was found that when the ionizing wavelength was 790Å, the observed drift velocities were in excellent agreement

with data obtained by other experimenters using techniques different from ours; however, when the spectral setting of the monochromator was 764Å, the drift velocities observed were by about a factor of two greater. Simultaneously, the ion density profile observed on the screen of the oscilloscope was no longer symmetric, but became skewed, indicating the presence of two groups of ions with different velocities. At the wavelength setting of 790Å (close to the threshold of N_2^+ formation) only ground state N_2^+ ions can be generated. At 764Å excitation to the first vibrational level is also possible. This channel would be significant if an appreciable fraction of the ions were formed by autoionization. The observation that two groups of ions are involved at 764Å makes evident that autoionization is significant and that N_2^+ ($v = 1$) ions are endowed with a higher mobility than N_2^+ ($v = 0$) ions.

The formation of N_4^+ occurs at both wavelengths. The rate coefficient for this reaction had been measured previously with the photoionization technique at 764Å. Third body kinetics were observed. This observation has been criticized as being inconsistent with a number of other data in the literature. In view of the participation of N_2^+ ($v = 1$) ions at 764Å it was considered necessary to re-investigate the process of N_4^+ formation at 790Å, where only ground state N_2^+ ions are initially present. The details of the results and their implications are given in the present section in the form of a paper submitted for publication in the Journal of Geophysical Research.

In a recent comment concerning a discussion[1] of atmosphere ion-neutral reaction rates, Varney[2] objected to listing the formation of N_4^+ via the association

$$N_2^+ + N_2 \rightarrow N_4^+ \qquad (1)$$

as a three body reaction, and he cited experimental results which indicated that it proceeds as a two body process. Specifically, the after glow data of Fite,et al;[11] the mass spectrometer results of Saporoschenko;[3] and a variety of drift experiments[4,5,6] have indicated a direct two-body association whereas the more recent photoionization mass spectrometer experiments by Warneck[2] and the low pressure electron impact mass spectrometer observations by Asundi, Schulz and Chantry[7] displayed third order kinetics. Since the discrepancy is serious, we have performed a new set of experiments with the photoionization technique, following the suggestions by Varney[8] that the parameter E/p, the ratio of the electric field strength to the pressure, be kept constant in the ion source so that the energy of the reacting ions remains unchanged. The new results and their implications are the topic of this note.

Initially, the former results with constant E and varying p were verified, using for the production of N_2^+ radiation centered at 764Å, as described previously.[2] Since this permits the production of vibrationally excited nitrogen ions, the new experiments were performed at 790Å, near the threshold of nitrogen ionization, where the formation of excited nitrogen ions is precluded. At 790Å the measured drift velocities of N_2^+ agreed well with those reported in the literature,[6,9] whereas the drift velocities at 764Å were by a factor of two higher, presumably due to the presence of a considerable portion of vibrationally excited nitrogen ions formed by autoionization. Rate coefficients for N_4^+ formation were determined at 790Å in a series of experiments for which E/p was held constant for various field strengths and pressures; and in another series of experiments for which the pressure was

varied while the field strength was held constant but differed for each set of values. All observations showed a pressure dependence of the derived bimolecular rate constant similar to that found previously,[2] thereby demonstrating third order kinetics. Moreover, the third order rate coefficients derived from all these experiments agree within the experimental error, the value being $k = (4.4 \pm 0.6) \times 10^{-29}$ cc^2/molecule^2 sec. Accordingly, the variation with pressure is due to the influence of the third body and not due to a variation with E/p in the region of relative field strengths covered ($8 < E/p < 33$ volt/cm/Torr). The new results, therefore, corroborate our previous conclusion that for the conditions employed in the photoionization mass spectrometer an equilibrium between N_2^+ and N_4^+ is not established.

The ionizing energies employed here in photoionizing nitrogen are in a region where corresponding electron impact experiments have demonstrated N_4^+ formation from neutral excited nitrogen via the process:

$$e + N_2 \rightarrow N_2^* + e \qquad (2)$$

$$N_2^* + N_2 \rightarrow N_4^+ + e \qquad (3)$$

occurring in addition to N_4^+ formation from N_2^+.[7,10]

In view of the knowledge that in the wavelength region 685Å - 850Å the absorption spectrum of nitrogen is at least partially discrete, and that photoionization efficiencies are less than unity, the formation of excited nitrogen molecules is certain to occur also in the present experiments. Although the excited states reached by UV radiation and by electron impact are not necessarily the same, it is clear that allowance must be made for the possibility of reaction (3) participating in the photoionization mass spectrometer experiments. However, no experimental evidence has been found for any

occurrence of the process. Specifically, no N_4^+ formation was detected at energies below, (i.e. at wavelengths above) the onset of N_2^+ formation - in contrast to the electron impact results, and approximately the same rate of N_4^+ formation as at 790Å was observed when the wavelength was set to 685Å, where the ionization efficiency is nearly unity. Thus, while reaction (3) cannot be entirely precluded, it does not appear to occur to a significant extent in the present experiments. It is concluded that the observed formation of N_4^+ is due predominantly to reaction (1) in its termolecular mode, in agreement with our earlier conclusion.[2]

There remains to explain the discrepancy arising from the various data in the respect to third or second order kinetics of N_4^+ formation. Evidently, this problem is connected with the observation that at high E/p values N_4^+ ions gain sufficient energy in the field to dissociate upon collision. Mass spectrometrically identified ion transients in drift tubes are nearly identical for N_2^+ and N_4^+ when E/p is high, demonstrating that a rapid equilibrium between the two species is achieved.[6,9] In low fields, however, the two ion transients are well separated even though a significant $N_2^+ - N_4^+$ conversion occurs. In this region, therefore, a rapid interchange is not operative. The low field region is well suited to studies of reaction (1) and in this region, the formation of N_4^+ is third body dependent. On the other hand, in the high field region, reaction (1) is in equilibrium with the dissociation of N_4^+, so that in this case the abundance of N_4^+ will depend only linearly on the nitrogen pressure. It appears that in those cases where bimolecular N_4^+ formation was deduced[3,6,11] the high field conditions favored equilibration of N_2^+ and N_4^+. The mass spectrometer results of Asundi, Schulz and Chantry[7] provide direct

evidence for such an interpretation.

2. Laboratory Measurements of VUV Photon Scattering Cross Sections for Selected Atmospheric Gases

For the discussion of laboratory measurements on the molecular scattering of VUV radiation by specific gases, it is convenient to express the phenomenon in the form of the following equation:

$$\Phi_\theta \, d\omega = \Phi \quad \frac{\pi^2 V (n^2-1)^2}{2 \lambda^4 N} \quad \frac{6}{(6 - 7\rho_n)} \left(1 + \cos^2 \theta + \rho_n \sin^2 \theta \quad d\omega\right) \quad (4)$$

In this equation, the term $\Phi_\theta \, d\omega$ represents the number of photons scattered per second into the solid angle, $d\omega$, observed at an angle, θ, to an incident unpolarized photon beam of intensity, Φ. In addition, N is the molecular number density, V represents the scattering volume, and λ the photon wavelength. The (n^2-1) term represents the refractive index of the gas, and ρ_n is the polarization factor of scattered light in excitation by unpolarized light. For the specific cases of $\theta = 90^o$ and $\theta = 54^o44'$, Equation (4) assumes the following forms:

$$\Phi_{90^o} \, d\omega = \Phi \left[\frac{\pi^2 V (n^2-1)^2}{2 \lambda^4 N}\right]\left[\frac{6 + 6\rho_n}{6 - 7\rho_n}\right] d\omega \, , \quad (5)$$

$$\Phi_{54^o} \, d\omega = \Phi \left[\frac{N V \sigma_s}{4\pi}\right] d\omega \, . \quad (6)$$

Thus, for the case of purely symmetric molecules (i.e., CH_4, $CC\ell_4$, etc.) and atoms (i.e., A, He, Kr, etc.) $\rho_n \equiv 0$ so that

$$\frac{\Phi_{54^o}}{\Phi_{90^o}} = \frac{4}{3} \quad (7)$$

In a detailed discussion given previously, (see Quarterly Progress Report #11 under NASA Contract No. NASW-1283, November, 1967) it was

demonstrated that the simple relationship shown in Equation (7) is convenient to employ as a calibration feature in the laboratory measurement of the ρ_n-values. Furthermore, these relationships can be employed as a convenient representation for comparing experimental measurements with available theoretical σ_s-values without prior knowledge of the individual ρ_n term.

For the cases wherein $\rho_n \neq 0$, the following expressions obtain:

$$\frac{\phi_{54^o}}{\phi_{90^o}} = \frac{4 + 2\rho_n}{3 + 3\rho_n} = R \tag{8}$$

and

$$\rho_n = \frac{3R - 4}{2 - 3R} \tag{9}$$

On this basis, then, it would be appropriate to design a scattering chamber wherein the $\phi 54/\phi 90$ - ratio could be measured in order to minimize any systematic error involved. At this point it is important to emphasize that this relationship holds only for the case where the incident radiation is completely unpolarized. However, owing to the fact that in the present experimental configuration a grating is involved, it turns out that the incident radiation is indeed polarized. Furthermore, the measurement of the degree and sense of polarization is difficult to ascertain experimentally in this VUV region. Thus, it would appear that this would constitute a significant barrier for acquiring laboratory σ_s and/or ρ_n-values. However, it will be demonstrated that on the basis of additional analysis described below this difficulty can be eliminated by employing a unique experimental configuration for the scattering chamber. Specifically, it will be demonstrated that to obtain σ_s-values without a prior knowledge of the ρ_n-value, scattered radiation should be observed in the unique position of $54^o44'$ with respect to a coordinate axis oriented such that the incident radiant energy is along the y-axis and at the same time the x or z-axis is parallel to the major or minor direction of polarization. Also, a second

observation performed at another angle yields the ρ_n-value itself.

For the present purpose it is convenient to express the total scattering cross section for radiant energy I_o incident on a volume element V or partical density N as follows:

$$\sigma_s = \frac{I}{I_o NV} \quad , \tag{10}$$

where I is the total radiant energy scattered. Experimentally, detectors can intercept only a small fraction of the total scattered radiant energy. Thus it is necessary to know the dependence of the scattered radiation on the angle of observation, on the anisotropy of the molecules, and on the degree of polarization of the incident radiant energy. In the following discussion the general expression for the angular distribution of the scattered radiant energy is developed. It will be shown that the average intensity $\overline{I}_s$ scattered per unit solid angle can be observed at a specific angle and is independent of the degree of polarization of the incident radiant energy. Thus $\sigma_s = 4\pi \overline{I}_s / I_o NV$. Further, it is shown that the normal depolarization factor ρ_n can be determined from the ratio of two measurements at specific angles such that it is unnecessary to know the degree of polarization of the incident radiant energy. This is important since most monochromators produce partially polarized radiant energy which varies with the wavelength and polarizers are not readily available in the vacuum UV without producing a series loss in intensity.[12-14]

If the incident radiant energy induces an electric moment p in a molecule then the radiant energy scattered per unit solid angle I_s in the direction θ with respect to the electric moment vector is given by

$$I_s = \frac{2\pi^3 c}{\lambda^4} p^2 \sin^2\theta \tag{11}$$

where λ is the wavelength of the incident radiant energy and c is the velocity of light. The induced electric moment is usually written as $p = \alpha E$, where α is called the polarizability of the molecule and E is the magnitude of the electric vector. With the units used here the radiant energy is equal to $(c/8\pi)E^2$. In general, the polarizability of a molecule depends on the direction of the incident beam in relation to the axis of symmetry of the molecule. If the electric vector of an incident plane polarized beam is parallel to one of these axes the induced moment along the axis vibrates parallel to the incident vector. If viewed at right angles to the incident beam and the electric vector the scattered radiant energy will also be plane polarized. However, if the electric vector is not parallel to any of the principal axes it will induce moments along each of the axes and the scattered radiant energy has been depolarized by the anisotropic molecules. Since the molecules will be oriented at random it is necessary to compute the average value of p^2 in order to determine the intensity of the radiant energy scattered.

Consider an incident beam of partially polarized radiant energy to be traveling along the y-axis of a cartesian coordinate system x, y, z with the principal direction of polarization in the z-direction and with the other planes of polarization distributed symmetrically about the z-axis. This is equivalent to two beams polarized in the x and z-directions with electric vectors E_x and E_z. Let the components of p along these axes be p_x, p_y, and p_z. The values of p_x^2, p_y^2, and p_z^2, are proportional to the intensity of that part of the scattered beam in which the vibrations are restricted to the x, y, and z directions, respectively. The average values of the components have

been calculated (see for example Bhagavantam[15]) and are given as follows in terms of the polarizabilities A, B, and C along the axes of symmetry of the molecule.

$$\bar{p}_x^2 = E_x^2 \left[\frac{3}{15}(A^2 + B^2 + C^2) + \frac{2}{15}(AB + BC + AC)\right] + E_z^2 \left[\frac{1}{15}(A^2 + B^2 + C^2 - AB-BC-AC)\right] \quad (12)$$

$$\bar{p}_y^2 = (E_x^2 + E_z^2) \left[\frac{1}{15}(A^2 + B^2 + C^2 - AB - BC - AC)\right] \quad (13)$$

$$\bar{p}_z^2 = E_z^2 \left[\frac{3}{15}(A^2+B^2+C^2) + \frac{2}{15}(AB+BC+AC)\right] + E_x^2 \left[\frac{1}{15}(A^2+B^2+C^2-AB-BC-AC)\right] \quad (14)$$

Defining the mean polarizability as $\alpha_o = \frac{1}{3}(A + B + C)$, the anisotropy of the molecule as $\gamma^2 = A^2 + B^2 + C^2 - AB - BC - AC$, $g = E_x/E_z$, and $E_o^2 = E_x^2+E_y^2$, we obtain

$$\bar{p}_x^2 = 3 E_o^2 \alpha_o^2 \left[\frac{2g - g\rho_n + \rho_n}{(1+g)(6-7\rho_n)}\right] \quad (15)$$

$$\bar{p}_y^2 = 3 E_o^2 \alpha_o^2 \left[\frac{\rho_n}{(6-7\rho_n)}\right] \quad (16)$$

$$\bar{p}_z^2 = 3 E_o^2 \alpha_o^2 \left[\frac{2 + g\rho_n - \rho_n}{(1+g)(6-7\rho_n)}\right] \quad (17)$$

where $\rho_n = 6\gamma^2/45\alpha_o^2 + 7\gamma^2)$. This value is called the normal depolarization factor and is zero when $\gamma^2 = 0$, that is, when the molecule is perfectly symmetrical. Physically, it is defined for incident unpolarized radiant energy as the ratio of the intensity of the scattered radiant energy polarized in the y-direction to that polarized in the z-direction when viewed along the x-axis. Thus, it can be obtained from the ratio of Eq. (13) to Eq. (14) placing $E_x = E_z$. The factor g is related to the degree of polarization P by the relation $P = (1-g)/(1+g)$.

The intensity of the scattered radiant energy per unit solid angle in the direction θ, η, and ψ (as shown in Fig. 1) is given by:

$$I_s(\theta,\eta,\psi) = \frac{2\pi^3 c}{\lambda^4} \left(\bar{p}_x^{\,2} \sin^2\theta + \bar{p}_y^{\,2} \sin^2\eta + \bar{p}_z^{\,2} \sin^2\psi \right)$$

$$= \frac{2\pi^3 c}{\lambda^4} \left(\bar{p}_x^{\,2} + \bar{p}_y^{\,2} + \bar{p}_z^{\,2} \right) - \left(\bar{p}_x^{\,2} \cos^2\theta + \bar{p}_y^{\,2} \cos^2\eta + \bar{p}_z^{\,2} \cos^2\psi \right) \tag{18}$$

But the sum of the direction cosines $\cos^2\theta + \cos^2\eta + \cos^2\psi = 1$.

Substituting for $\cos^2\eta$ in Equation (18),

$$I_s(\theta,\eta,\psi) = \frac{2\pi^3 c}{\lambda^4} \left(\bar{p}_x^{\,2} + \bar{p}_z^{\,2} \right) + \left(\bar{p}_y^{\,2} - \bar{p}_z^{\,2} \right) \cos^2\theta + \left(\bar{p}_y^{\,2} - \bar{p}_x^{\,2} \right) \cos^2\psi \tag{19}$$

That is, I_s is of the form

$$I_s(\theta,\eta,\psi) = \underline{a} + \underline{b} \cos^2\theta + \underline{c} \cos^2\psi \quad , \tag{20}$$

where from Eqs. (15), (16), and (17),

$$\underline{a} = \left(\frac{2\pi}{\lambda}\right)^4 I_o \alpha_o^{\,2} \frac{6}{(6-7\rho_n)}$$

$$\underline{b} = \left(\frac{2\pi}{\lambda}\right)^4 I_o \alpha_o^{\,2} \frac{6(\rho_n-1)}{(1+g)(6-7\rho_n)}$$

$$\underline{c} = \left(\frac{2\pi}{\lambda}\right)^4 I_o \alpha_o^{\,2} \frac{6g(\rho_n-1)}{(1+g)(6-7\rho_n)} \quad ,$$

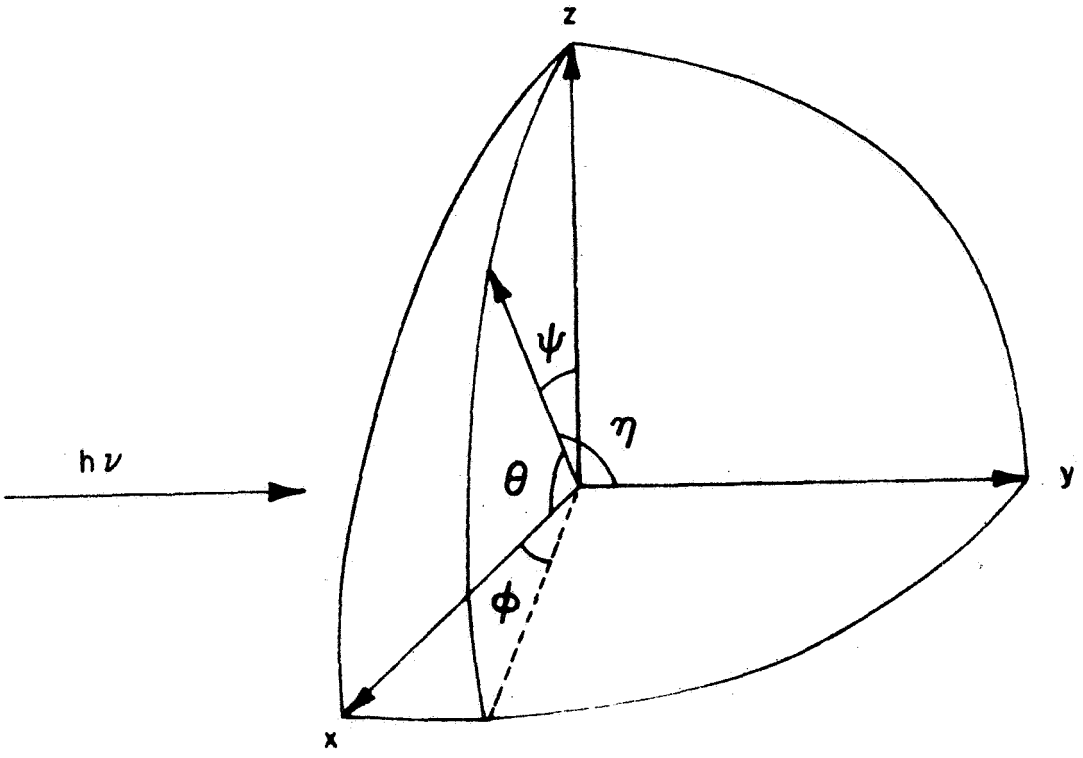

Figure 1. Radiant energy scattered in the direction θ, η, and ψ. The incident radiation is along the y-axis.

where $I_o = E_o^2 (c/8\pi)$ is the total incident radiant energy.

The average radiant energy $\bar{I}_s$ scattered per unit solid angle can be obtained from Eq. (20) as follows:

$$\bar{I}_s \frac{\int_0^{2\pi} (\underline{a} + \underline{b} \cos^2\theta + \underline{c} \cos^2\psi) \, d\omega}{\int_0^{2\pi} d\omega}$$

where the incremental solid angle $d\omega = \sin\psi \cdot d\psi \cdot d\phi$ and ϕ is the angular direction of the scattered radiant energy in the x - y plane. From Fig. 1 it can be seen that $\cos\theta = \sin\psi \cdot \cos\phi$. Substituting the values for $d\omega$ and $\cos\theta$ into the integral above and integrating, we obtain:

$$\bar{I}_s = \underline{a} + \underline{b}/3 + \underline{c}/3. \tag{21}$$

That is

$$\bar{I}_s = 32 \, I_o \left(\frac{\pi}{\lambda}\right)^4 \alpha_o^2 \frac{(2 + \rho_n)}{(6 - 7\rho_n)} \tag{22}$$

Equating Eqs. (20) and (21) it is seen that $\bar{I}_s$ is obtained when $\cos^2\theta = \cos^2\psi = 1/3$. That is when

$$\theta = \psi = \eta = 54^o44'. \tag{23}$$

From Eq. (22) α_o^2 is proportional to the scattered intensity and hence to the scattering cross section. Since $\sigma_s = 4\pi \bar{I}_s/(I_o NV)$, we have,

$$\sigma_s = \left[\frac{128\ \pi^5\ \alpha_o^2}{\lambda^4\ NV}\right] \frac{(2 + \rho_n)}{(6 - 7\rho_n)} \tag{24}$$

Thus the general expression for the angular distribution of the scattered radiant energy in terms of σ_s rather than α_o^2 is given by,

$$I_s(\theta, \eta, \psi) \quad I_o\sigma_s \frac{3NV}{4\pi} \frac{1}{(2 + \rho_n)} \quad \left[1 + \frac{(\rho_n - 1)}{(1 + g)} \cos^2\theta + g \frac{(\rho_n - 1)}{(1 + g)} \cos^2\psi\right] \tag{25}$$

It should be noted than when $\theta = \eta = \psi = 54^o44'$ the scattered intensity I_s is equal to the average intensity of the scattered radiant energy and is independent of ρ_n and g. However, if I_s is observed at angles such that $\theta = \psi$ then I_s is independent of g.

In measuring the Rayleigh scattering cross section of a molecule the scattered radiation should be observed in the direction $54^o44'$ with respect to a coordinate axis oriented such that the incident radiant energy is along the y-axis and at the same time the x or z-axis is parallel to the major or

minor direction of polarization. This is the direction in which the intensity scattered per solid angle is equal the average intensity scattered. The intensity is also independent of the degree of polarization of the incident radiation and depends simply on the total scattering cross section σ_s without requiring specific knowledge of the normal depolarization factor ρ_n as is required when any other angle of observation is used. To obtain the value of ρ_n a second observation must be made at any other angle except $54^o44'$. If a measurement is made with the additional constraint $\theta = \psi$ the scattered signal is independent of the degree of polarization of the incident radiant energy. From the ratio of the two measurements ρ_n can be found. For example,

$$\frac{I_s\ (54^o44')}{I_s\ (\theta = \psi = 45^o)} = \frac{2(2 + \rho_n)}{3(1 + \rho_n)} \qquad (26)$$

This is of course true for each of the eight quandrants of the sphere centered on the scattering volume element. If the volume elements observed at the two different angles are not equal their ratio can be determined by repeating the experiment with a spherically symmetrical atom, such as argon, where $\rho_n=0$. On the basis of this analysis an appropriate scatter chamber is currently being designed and fabricated.

3. VUV Electron Spectroscopy of Atmospheric Gases

During the current quarter the photoelectron spectra of NO, CO and CO_2 have been obtained at wavelengths of 469.8Å (26.39eV) and 416.2Å (29.79eV). The techniques employed have been described previously[16] so that no detailed description is given herein.

For CO and CO_2 no new ionization potentials were observed at least up to the limiting photon energy (29.79eV). However, for the case of NO a new higher ionization potential was observed at 21.57eV although no evidence was found for the α-series at 14.23eV as reported by Tanaka[17] (an ionization potential was found at 15.52eV).

These new results are the subject matter of a letter entitled "Higher Ionization Potentials of Nitric Oxide" (J. A. R. Samson) which has been submitted for publication in the Physics Letters. The material contained in this letter is summarized below.

The measured retarding potential curve of nitric oxide is shown in Figure 2. The ionizing radiation was an Ar IV line of wavelength 462Å (26.84eV) produced by a low pressure condensed spark discharge in a capillary and dispersed by the GCA McPherson one-half meter Seya type monochromator. The band pass of the monochromater was 1Å (equivalent to 58mV at 462Å).

The various steps in the curve correspond to ionization potentials of NO. Considerable unresolved vibrational structure occurs between 15.7 and 19.5eV. The energy scale was calibrated using the first ionization potential of NO as 9.266eV as determined spectroscopically by Dressler and Miescher,[18] and also by mixing some helium to the nitric oxide gas. The

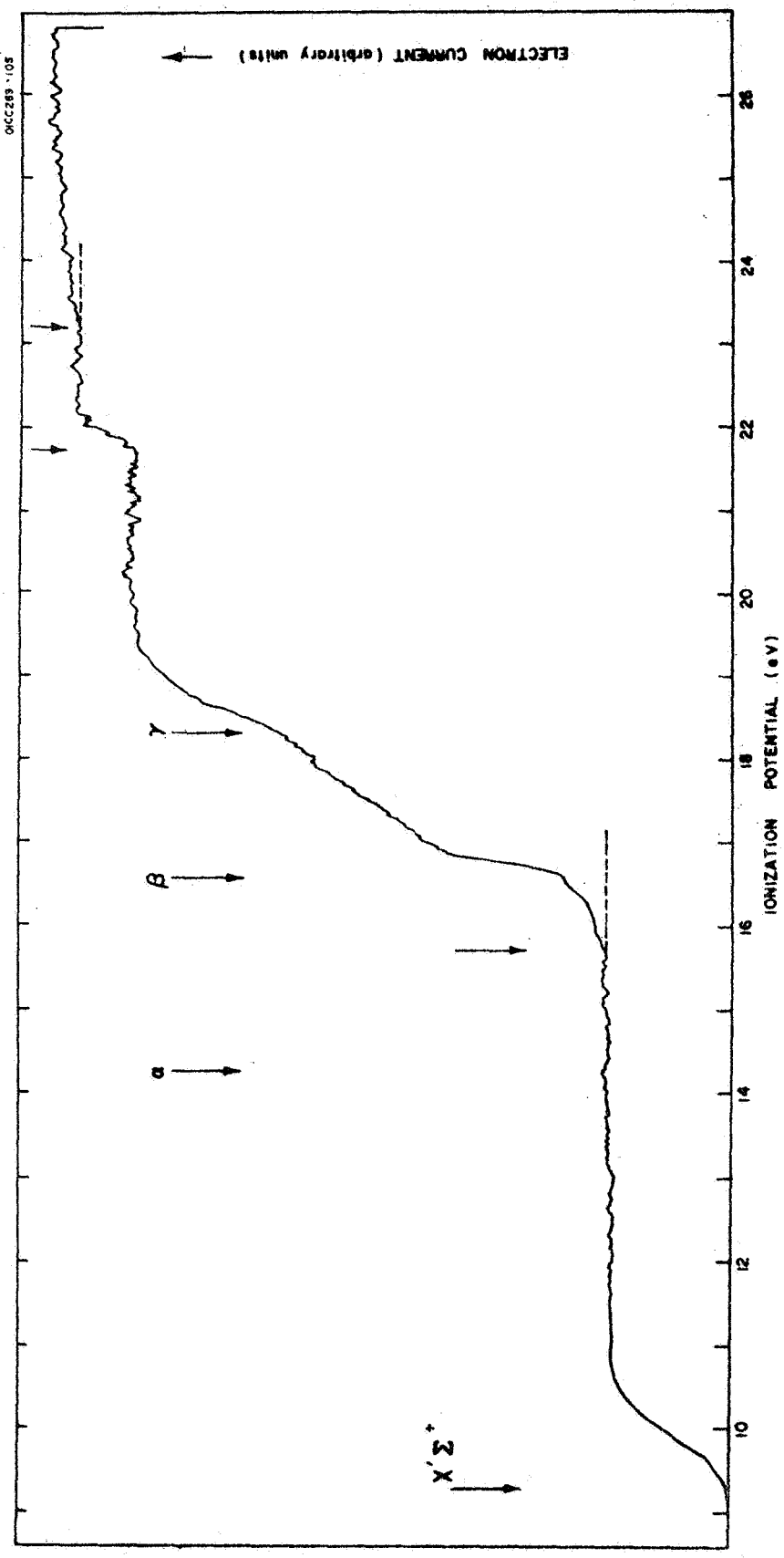

Figure 2. Electron energy spectrum of NO ionized by photons of 26.84 eV (462Å). The labeled arrows represent ionization potentials obtained spectroscopically.

helium gave a step at 24.58eV corresponding to its ionization potential. States corresponding to the Tanaka β and γ-series limits are observed at the appropriate energies. No state is observed at the α-series limit (14.15eV).[17] However, a level is observed at 15.67eV. This level has also been seen by others using photoelectron spectroscopy with the 584Å line (21.22eV).[19-21] It has been suggested that the transition probability for ionizing a state at the α-series limit could be exceedingly small at 584Å and hence not observed.[22] However, in the present work a search for a step in the retarding potential curve at the α-series limit was made at a variety of wavelengths shorter than 834Å (14.87eV), but none was found. It would appear, therefore, that the interpretation of the α-series as Rydberg terms leading to an excited state NO^+ is incorrect.

From the data in Figure 2, it is evident that a new, previously unreported ionization potential is observed at 21.72eV and a weaker one at 23.1eV. No other excited states were observed up to the limit of the present observations, namely, 30eV. An ionization potential at approximately 22eV has recently been observed by Price.[21]

4. Absorption and Photoionization Cross Sections for $\lambda\lambda < 500$Å

To perform studies of the interaction of radiation with a planetary gas at wavelengths below 500Å (task item 4) it is necessary to use a grazing incidence vacuum monochromator with a suitable light source. During the current quarter the first spectra were obtained on the VUV grazing incidence monochromator designed and constructed under the present program. Details of its operational parameters and a reproduction of the spectrum of atomic nitrogen is given in this report.

The construction of the monochromator was based on that described by Vodar.[23] The principle of operation is as follows (see Figure 3):

The light source is maintained at a fixed distance from the grating and the radiation is incident at a fixed angle of incidence. To scan the wavelength the grating moves along the linear track towards the exit slit while the light source is constrained to follow the track joining the entrance and exit slits. Because the source and grating distance is fixed, the grating and light source must be free to rotate about their respective centers (that is, the grating center and the entrance slit). The wavelength λ is then given by the distance ℓ separating the grating and the exit slit according to the following relation

$$\lambda = d \left[\sin \alpha - (1 - \ell^2/R^2)\right]^{1/2} . \qquad (27)$$

The constructional parameters were as follows:

$$R = 2.2176 \text{ meters}$$

$$1/d = 600 \text{ lines/mm}$$

$$\alpha = 84^{\circ}$$

$$\text{Blaze angle} = 2^{\circ}\ 14'$$

Blaze wavelength

$$\text{at } \alpha = 84^{\circ} = 169\text{Å}$$

$$\ell \text{ at } 0\text{Å} = 9.126''$$

A photograph of the finished instrument is reproduced from a previous report for convenience and completeness and is shown in Figure 4. The problem of moving parts under vacuum was solved by the use of stainless

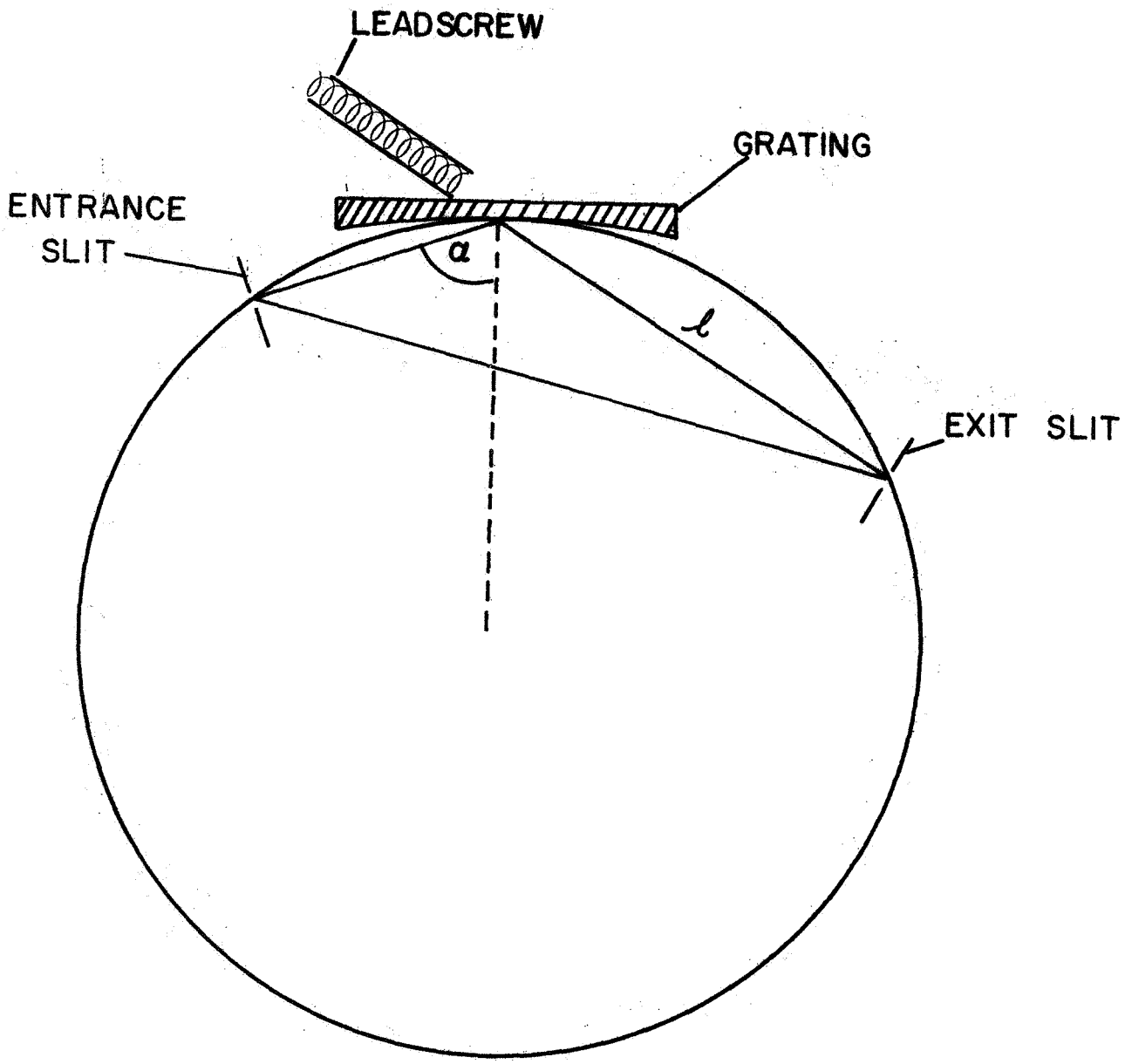

$$\lambda = d\,(\,\mathrm{SIN}\alpha - \sqrt{1-\ell^2/R^2}\,)$$

Figure 3. Schematic diagram of the Vodar-type grazing incidence monochromator. Wavelength identification is obtained from the relation:

$$\lambda = [\sin\alpha - (1-\ell^2/R^2)^{\frac{1}{2}}].$$

steel bellows which were capable of expanding and contracting over a total distance of 17". The bellows can be seen in Figure 4. The sagging of the bellows occurs when the instrument is at atmospheric pressure, but under vacuum conditions the bellows becomes straight and usable.

The instrument is capable of covering the wavelength range from 0 to 600Å. At 0Å the dispersion of the instrument is 20Å/inch in terms of a movement along ℓ, whereas at 584Å the dispersion is 50Å/inch. With slit widths of 40 microns a wavelength resolution of 0.4Å has been obtained over the full range of the instrument.

The various light sources in use at GCA were studied for their short wavelength capability. An immediate discovery was the fact that the important He I 304Å line was obtained with excellent intensity from our standard DC glow discharge lamp. In fact, the absolute intensity at the exit slit was measured and found to be 2.5×10^8 photons/sec for 40 micron wide slits.

The high voltage spark discharge light source was found to produce a dense line spectrum down to 129Å. The particular lines produced depends on the gas used in the source. Usually N_2, Ar, and O_2 are used. The discharge is so energetic that it dissociates the molecules and produces a line spectrum characteristic of the atoms only. Typically, lines of N IV and O VI are observed. Figure 5 shows a section of the spark spectrum of the source when N_2 is used. The shortest useful line to be observed was an oxygen impurity line O VI at 209.872Å. In the figure the amplitude of the photomultiplier dark current is shown. This background current is of course absent when the ion chamber is used to measure cross-sections.

From the measured absolute intensities it is clear that this instrument will be suitable for use with the photoelectron spectrometer for

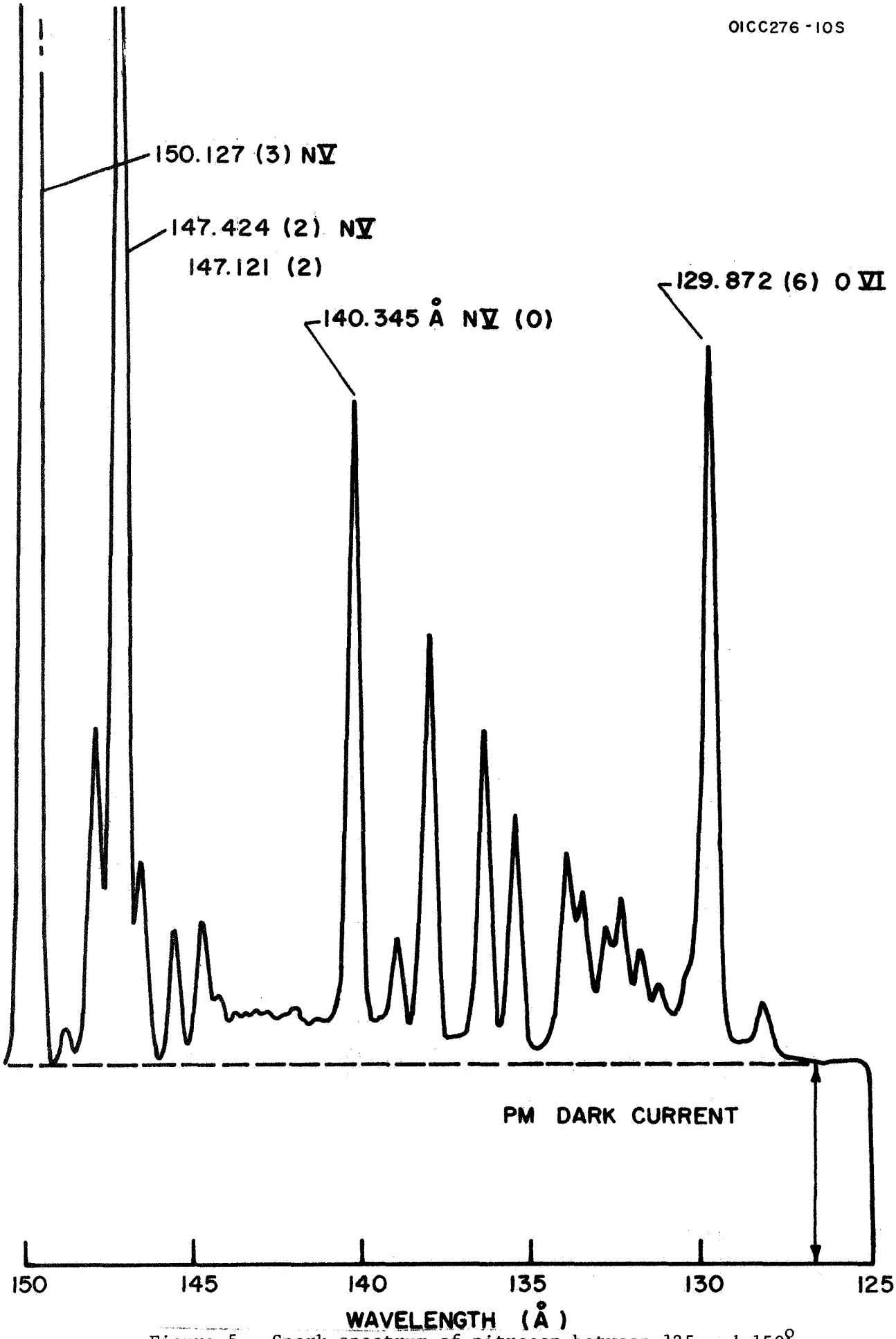

Figure 5. Spark spectrum of nitrogen between 125 and 150Å.

measuring higher ionization potentials. During the next quarter it is planned to mount the photoelectron spectrometer onto the exit slit of the grazing incidence monochromator.

B. THEORETICAL STUDIES

In accordance with the subject work statement, it is required to perform the following theoretical studies: (1) calculate photon scattering cross sections for $\lambda\lambda < 2500\text{Å}$, (2) suggest, evaluate and determine the feasibility of performing definitive experiments related to planetary atmospheres, (3) examine the quantitative effects of electron cooling in a planetary atmosphere, (4) calculate cross sections associated with ion cooling involving the fine structure bands of atomic oxygen as well as the rotational excitation of atmospheric molecules, (5) evaluate the role of meteoric debris in planetary atmospheres, and (6) perform calculations on the nature and intensity of VUV airglow in planetary atmospheres owing to EUV-produced photoelectrons.

The completion of task items 3 and 4 has been previously reported (see Quarterly Progress Report #1) and the results are discussed in a paper entitled "The Effect of Oxygen Cooling on Ionospheric Temperatures", (A. Dalgarno, et al) which has been submitted for publication in Planetary and Space Sciences.

During the current reporting period task item 1 has been completed; the results, given below in subsection 1 also appear in the form of a paper entitled "Dipole Properties of Molecular Hydrogen" (G. A. Victor and A. Dalgarno) which has been submitted for publication in the Journal of Chemical Physics. Finally, additional effort has been given toward completing task item 2 wherein a Martian Lander experiment is defined and evaluated in terms of its scientific potential; this is the subject matter of subsection 2 below.

1. VUV Photon Scattering Cross Sections for Hydrogen for $\lambda\lambda < 2500\text{Å}$

Approximate variational calculations[24] of various dipole

properties of molecular hydrogen have been carried out as a function of the wavelength of the incident radiation. Because of inadequacies in the representation of the unperturbed and perturbed molecular wavefunctions, the calculations fail for wavelengths less than about 2500Å. Experimental data on the oscillator strength distributions of molecular hydrogen, supplemented by refractive index data and sum rules, can be used to construct a model of the complete dipole spectrum which accurately reproduces dipole properties for wavelengths greater than about 1150Å. The procedures have been applied successfully in earlier work on the inert gases and molecular hydrogen[25] and molecular nitrogen,[26] though no distinction is there made between parallel and perpendicular transitions. Among the properties which may be investigated are the parallel and perpendicular dynamic dipole polarizibilities, the molecular anisotropy, the refractive index, the Verdet constant, the Rayleigh scattering cross section, and the Rayleigh depolarization factor. The model spectrum can also be used to calculate the tensor components of the van der Waals coefficient for a pair of interacting hydrogen molecules and to calculate the average excitation energy that controls the absorption of fast charged particles in hydrogen gas.

Dipole oscillator strengths have been determined from measurements of energy loss of fast electrons at different scattering angles by Lassettre and Jones,[27] by Geiger,[28] and by Geiger and Topschowsky.[29] The more recent measurements were taken with a resolution of about .007eV and show vibrational structure in the Lyman and Werner band systems and in higher terms. Dipole oscillator strengths have also been derived from measurements of radiative lifetimes.[30] Refractive index data between 1855Å and

5462Å are available[31] and Bridge and Buckingham[32] have measured the Rayleigh depolarization factor for scattering of laser light at 6328Å. The experimental values of wavelengths for the hydrogen molecular spectrum are listed by Dieke.[33]

The parallel dipole oscillator strength from a state Φ_o with energy E_o to a state Φ_n with energy E_n is defined by

$$f_n^{\parallel} = \frac{2(E_n - E_o)}{3} \left| \left\langle 0 \left| \sum_{i=1}^{N} z_i \right| n \right\rangle \right|^2, \tag{28}$$

where all quantities are in atomic units and z_i is the z component of the position vector of the i^{th} electron of the N electron system where the coordinate system is referred to the midpoint of the nuclear axis with the z axis along the nuclear axis. The perpendicular dipole oscillator strength is defined by

$$f_m^{\perp} = \frac{4(E_m - E_o)}{3} \left| \left\langle 0 \left| \sum_{i=1}^{N} x_i \right| m \right\rangle \right|^2 \tag{29}$$

where x_i is the x component in the same coordinate system.

The parallel component of the dynamic dipole polarizibility tensor at a frequency ω for the state Φ_o is given by

$$\alpha_{zz}(\omega) = \alpha_{\parallel}(\omega) = 3 \sum_n \frac{f_n^{\parallel}}{(E_n - E_o)^2 - \omega^2} \tag{30}$$

and the perpendicular component is given by

$$\alpha_{xx}(\omega) = \alpha_{\perp}(\omega) = \frac{3}{2} \sum_m \frac{f_m^{\perp}}{(E_m - E_o)^2 - \omega^2} \tag{31}$$

where the summations over n and m in (30) and (31) are over all states,

including the continuum, for which the respective oscillator strengths do not vanish. The refractive index is given by

$$n - 1 = 2\pi N\alpha(\omega) \tag{32}$$

where N is Avogadro's number and $\alpha(\omega)$ is the trace

$$\alpha(\omega) = \frac{2\alpha_{\perp}(\omega) + \alpha_{\parallel}(\omega)}{3} \quad . \tag{33}$$

The anisotropy, $\gamma(\omega)$ is defined by

$$\gamma(\omega) = \alpha_{\parallel}(\omega) - \alpha_{\perp}(\omega). \tag{34}$$

If we introduce the summations

$$S^{\parallel}(k) = 3\sum_{n} f_n^{\parallel} (E_n - E_o)^k,$$

$$S^{\perp}(k) = \frac{3}{2}\sum_{m} f_m^{\perp} (E_m - E_o)^k$$

and

$$S(k) = \frac{2\,S^{\perp}(k) + S^{\parallel}(k)}{3} \tag{35}$$

the oscillator strength sum rule may be written

$$S^{\parallel}(0) = S^{\perp}(0) = S(0) = N \tag{36}$$

We replace the actual oscillator strength distributions in (30) and (31) by model oscillator strength distributions in which only a finite number of terms are retained:

$$\alpha_{\parallel}(\omega) = \sum_{i=1}^{M_{\parallel}} \frac{a_i^{\parallel}}{\tilde{\omega}_i^{\parallel 2} - \omega^2}$$

$$\alpha_{\perp}(\omega) = \sum_{i=1}^{M_{\perp}} \frac{a_i^{\perp}}{\tilde{\omega}_i^{\perp 2} - \omega^2} \tag{37}$$

The experimental Franck-Condon factors[28] for the Lyman ($X\ ^1\Sigma_g^+ - B\ ^1\Sigma_u^+$) band system were used to construct the first 16 coefficients a_i. Four additional terms were added to (37) making $M_{\parallel} = 20$. The additional values were initially taken from variational calculations[24] based on the Weinbaum wavefunction. Initial values of a_i were chosen similarly from the experimental data on the Werner ($X\ ^1\Sigma_g^+ - C\ ^1\Pi_u$) band system.[28,33] The first 9 excited vibrational states were included, together with 4 additional terms from the variational calculations,[24] making $M_{\perp} = 13$. The values of the Werner and Lyman band system oscillator strengths, and the initial values of a_i, $\tilde{\omega}_i$, a_i, $\tilde{\omega}_i$ taken from the variational calculations were then adjusted to best fit the refractive index data,[31] subject to exactly reproducing the sum rule (36) and the measured anisotropy[32] at 6328Å. The resulting model oscillator strength distribution reproduces the dynamic polarizibility values derived from the measurements of the refractive index[31] from 5462Å to 1855Å to at worst 0.2% and at most wavelengths, to within 0.1%. Parameters for our final model spectrum are given in Table I. Electron scattering data[28] yield a value of 0.25 ± 0.04 for f_B and of 0.31 ± 0.04 for f_C, the oscillator strengths of the Lyman and Werner bands respectively while our model distributions give 0.30 for f_B and 0.35 for f_C. Browne[34] computed a theoretical value of 0.35 for f_C and Ehrenson and Phillipson[35] a theoretical value of 0.27 for f_B. The refractive index data at small wavelengths cannot be accurately reproduced by value of f_B and f_C much below 0.30 and 0.35 respectively.

Values of the dynamic dipole polarizibility and refractive index for molecular hydrogen at selected wavelengths, derived from the model oscillator strength spectrum, are compared in Table II with the experimental data.

TABLE I

Constants for the Model Molecular Hydrogen Oscillator Strengths

$a_i^{\parallel}$	$\omega_i^{\parallel}$	$a_i^{\perp}$	$\omega_i^{\perp}$
0.0081	0.41096	0.07508	0.45173
0.0144	0.41697	0.12180	0.46223
0.0297	0.42281	0.11655	0.47213
0.0459	0.42849	0.07612	0.48142
0.0648	0.43401	0.04882	0.49014
0.0774	0.43939	0.02835	0.49829
0.0819	0.44462	0.01838	0.50581
0.0882	0.44970	0.01628	0.51272
0.0882	0.45464	0.01418	0.51904
0.0864	0.45943	0.35245	0.57621
0.0801	0.46410	0.57418	0.73544
0.0630	0.46863	0.46842	1.16207
0.0558	0.47300	0.08940	2.89711
0.0459	0.47728		
0.0369	0.48142		
0.0315	0.48539		
0.4167	0.57678		
0.4326	0.67414		
0.2491	1.07059		
0.0034	2.28982		

TABLE II

Dynamic dipole polarizibility in units of a_o^3 and refractive index of H_2

	Theory				Experiment[a]			
λ(Å)	α	$\alpha_\perp$	$\alpha_\parallel$	$(n-1)^*$	α	$\alpha_\perp$	$\alpha_\parallel$	$(n-1)^*$
∞	5.450	4.774	6.803	1.364(-4)	5.437	--	--	1.360(-4)
6328.0	5.554	4.857	6.949	1.390(-4)	5.554	4.86	6.95	1.390(-4)
5462.3	5.591	4.886	7.001	1.399(-4)	5.582	--	--	1.396(-4)
4359.6	5.675	4.952	7.120	1.420(-4)	5.667	--	--	1.418(-4)
4079.0	5.708	4.979	7.167	1.428(-4)	5.701	--	--	1.426(-4)
4047.7	5.713	4.982	7.173	1.429(-4)	5.705	--	--	1.427(-4)
3342.4	5.845	5.087	7.361	1.462(-4)	5.840	--	--	1.461(-4)
2968.1	5.963	5.179	7.529	1.492(-4)	5.960	--	--	1.491(-4)
2753.6	6.056	5.253	7.663	1.515(-4)	6.055	--	--	1.515(-4)
2535.6	6.182	5.351	7.843	1.547(-4)	6.183	--	--	1.547(-4)
2379.1	6.299	5.443	8.012	1.576(-4)	6.303	--	--	1.577(-4)
2302.9	6.368	5.496	8.111	1.593(-4)	6.384	--	--	1.594(-4)
1990.5	6.766	5.803	8.692	1.693(-4)	6.771	--	--	1.694(-4)
1935.8	6.865	5.879	8.837	1.718(-4)	6.868	--	--	1.718(-4)
1862.7	7.017	5.995	9.062	1.756(-4)	7.017	--	--	1.755(-4)
1854.6	7.035	6.009	9.089	1.760(-4)	7.035	--	--	1.760(-4)
1700.0	7.471	6.337	9.739	1.869(-4)	--	--	--	--
1600.0	7.872	6.636	10.354	1.970(-4)	--	--	--	--

λ(Å)	α	$\alpha_\perp$	$\alpha_\parallel$	$(n-1)^*$	α	$\alpha_\perp$	$\alpha_\parallel$	$(n-1)^*$
1500.0	8.431	7.045	11.204	2.109(-4)	--	--	--	---
1400.0	9.262	7.638	12.509	2.317(-4)	--	--	--	---
1300.0	10.625	8.573	14.730	2.658(-4)	--	--	--	---
1215.7	12.765	9.933	18.428	3.194(-4)	12.8	--	--	3.05 (-4)

* The number in parenthesis is the power of ten by which the entry is to by multiplied

(a) The experimental numbers are derived from the following sources: $\lambda = \infty$, reference (38); $\lambda = 6328$, reference (32) $\lambda = 1215.7$ (Lyman α), reference (36) modified as described in the text; all other values, reference (31).

The agreement at Lyman alpha (1215.7Å) between the value reported by Gill and Heddle,[36] the present theoretical result, and an earlier theoretical estimate[37] of 12.8 a_o^3 is excellent. However, Gill and Heddle used a depolarization factor of 0.014 in the analysis of their data. The use of our more precise prediction of 0.055 modifies their value for $|n-1|$ from 3.20×10^{-4} to 3.05×10^{-4} and their value of the average dipole polarizibility of 12.8 a_o^3 to 12.2 a_o^3.

If the rotational structure is not resolved, and the incident wavelength is not near a resonance wavelength, the Rayleigh scattering cross section is given by[37]

$$Q_{Ray}(\lambda) = \frac{128\pi^5}{9\lambda^4}\left\{3\alpha(\omega)^2 + \frac{2}{3}\gamma(\omega)^2\right\} \tag{38}$$

and the Rayleigh depolarization factor for unpolarized incident light is given by

$$\rho_{Ray}(\omega) = \frac{6\gamma(\omega)^2}{45\gamma(\omega)^2 + 7\gamma(\omega)^2} \tag{39}$$

Values of the molecular anisotropy $\gamma(\omega)$, the Rayleigh scattering cross section $Q_{Ray}(\omega)$, and the Rayleigh depolarization factor $\rho_{Ray}(\omega)$ for selected wavelengths are given in Table III. The theoretical values at Lyman alpha (1215.7Å) are 8.495 a_o^3, 2.35×10^{-24} cm^2, and 0.0552 respectively, while the estimate of reference (37) gives 2.1×10^{-24} cm^2 for Q_{Ray}. At shorter wavelengths, the anisotropy $\gamma(\omega)$ increases more rapidly than the polarizibility $\alpha(\omega)$, so that the depolarization factor $\rho_{Ray}(\omega)$ increases markedly above its long wavelength limit of about 0.018 to a value of 0.055 at Lyman alpha, where it significantly modifies the interpretation of measurements of photon scattering.[36]

The Verdet constant for molecular hydrogen is closely approximated by the Becquerel formula[39]

$$V = 1.007 \times 10^6 \lambda \frac{dn}{d\lambda} \tag{40}$$

TABLE III

The anisotropy, Rayleigh cross section and depolarization factor, and the Verdet constant (in units of microminutes/oersted-centimeter-atmosphere) for molecular hydrogen

$\lambda(\mathring{A})$	$\gamma(a_o^3)$	ρ_{Ray}	$Q_{Ray}(cm^2)$	V
∞	2.029	0.0181	0	0
6328.0	2.092	0.0185	5.69(-28)	5.35
5462.3	2.115	0.0187	1.04(-27)	7.29
4359.6	2.168	0.0190	2.64(-27)	11.8
4079.0	2.188	0.0192	3.48(-27)	13.7
4047.7	2.191	0.0192	3.60(-27)	13.9
3342.4	2.274	0.0197	8.11(-27)	21.6
2968.1	2.350	0.0202	1.36(-26)	28.6
2753.6	2.410	0.0206	1.89(-26)	34.5
2535.6	2.492	0.0211	2.75(-26)	42.6
2379.1	2.569	0.0216	3.68(-26)	50.6
2302.9	2.615	0.0219	4.29(-26)	55.3
1990.5	2.889	0.0236	8.70(-26)	85.3
1935.8	2.958	0.0241	1.00(-25)	93.2
1862.7	3.067	0.0247	1.22(-25)	106.
1854.6	3.080	0.0248	1.25(-25)	108.
1700.0	3.401	0.0268	2.00(-25)	147.
1600.0	3.710	0.0286	2.84(-25)	188.
1500.0	4.159	0.0313	4.24(-25)	253.
1400.0	4.871	0.0354	6.80(-25)	363.
1300.0	6.158	0.0426	1.22(-24)	591.
1215.7	8.495	0.0552	2.35(-24)	1070.

in units of microminutes/oersted-centimeter-atmosphere. Values of the Verdet constant at various wavelengths calculated from the model oscillator strength distributions are given in Table III. Our values of 7.29 and 11.8 at 5462Å and 4360Å respectively agree with the measured values[39] of 7.06 and 11.4 to within the experimental error.

The oscillator strength moment functions $S^{\parallel}(k)$, $S^{\perp}(k)$ and $S(k)$, defined by equation (35), provide useful information on molecular structure, and many properties of interest can be expressed in terms of them. Values of the moment functions for molecular hydrogen, calculated from the model spectrum are given in Table IV. Values based on the accurate variational calculations of Kolos and Wolniewicz[40] are given for comparison. The values of $S^{\parallel}(+2)$, $S^{\perp}(+2)$ and $S(+2)$ are not of high accuracy because of inadequacies at the large frequency part of the spectrum. The values of $S^{\parallel}(0)$, $S^{\perp}(0)$ and $S(0)$ are exact, of course, because the model spectrum was constructed subject to this constraint. The relations[41]

$$
\begin{aligned}
S^{\parallel}(-1) &= 2 \left\langle \Phi_o \mid (z_1 + z_2)^2 \mid \Phi_o \right\rangle \\
S^{\perp}(-1) &= 2 \left\langle \Phi_o \mid (x_1 + x_2)^2 \mid \Phi_o \right\rangle \\
S^{\parallel}(-2) &= \alpha^{\parallel} \quad (\omega = 0) \\
S^{\perp}(-2) &= \alpha^{\perp} \quad (\omega = 0)
\end{aligned}
\tag{41}
$$

give the moments in terms of expectation values of certain operators with respect to the ground state wavefunction Φ_o. Since the values of these operators are a function of internuclear separation, integration with respect to the appropriate vibrational wavefunction for the ground state and averaging over rotational states corresponding to the temperature of interest is necessary. Values of $S^{\parallel}(-2)$, $S^{\perp}(-2)$ and $S(-2)$ determined by Kolos and Wolniewicz,[40] where vibrational and rotational averaging was effected, agree very well with

TABLE IV

Moment functions of the dipole oscillator strength distribution for molecular hydrogen*

k	$S^{\parallel}(k)$	$S^{\perp}(k)$	$S(k)$
+2	0.82	1.93	1.56 (3.693)
+1	1.214	1.674	1.520 (1.704)
0	2.000	2.000	2.000
-1	3.580 (3.541)	2.913 (2.826)	3.135
-2	6.803 (6.786)	4.774 (4.750)	5.450 (5.429)
-3	13.48	8.433	10.12
-4	27.55	15.67	19.63

* The values in parenthesis are based on the accurate variational calculations of Kolos and Wolniewicz.[40]

the corresponding model spectrum values. The agreement is less good for $S^{\parallel}(-1)$, where only vibrational averaging was done, and for $S^{\perp}(-1)$, where the operators were evaluated only at the equilibrium separation.

The important molecular parameter in the Bethe[42] theory of the stopping of high velocity charged particles in molecular hydrogen gas is defined by the sum

$$\ell n I = \frac{\sum_n f_n^{\parallel} \ell n (E_n - E_o) + \sum_m f_m^{\perp} \ell n (E_m - E_o)}{2} \qquad (42)$$

The mean excitation energy I is found to be 18.6eV, compared to previous theoretical estimates of 18.4eV,[43] and 19.5eV.[44]

The long-range dispersion energy between two hydrogen molecules depends upon the orientation of the molecular axes. Using the geometry shown in Fig. 6, the long-range interaction energy is[45]

$$\begin{aligned} V = -R^{-6} \Big\{ & (C_{\parallel,\parallel} + C_{\perp,\perp} - 2C_{\parallel,\perp}) \\ & \left[\sin\theta_a \sin\theta_b \cos(\Phi_a - \Phi_b) - 2\cos\theta_a \cos\theta_b \right]^2 \\ & + 3(C_{\parallel,\perp} - C_{\perp,\perp}) \cos^2\theta_a \\ & + 3(C_{\parallel,\perp} - C_{\perp,\perp}) \cos^2\theta_b \\ & + (2C_{\parallel,\perp} + 4C_{\perp,\perp}) \Big\} \end{aligned} \qquad (43)$$

According to the Casimir-Polder[46] formula, and simple geometry, the constants $C_{\parallel,\parallel}$, $C_{\parallel,\perp}$, and $C_{\perp,\perp}$ can be expressed as simple linear combinations of the integrals

$$\frac{3}{\pi} \int_0^{\infty} \alpha_{\parallel} (i\omega) \, \alpha_{\parallel}(i\omega) \, d\omega \quad ,$$

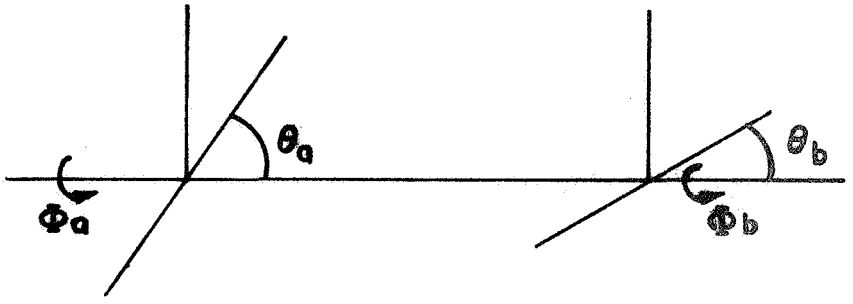

Figure 6. Geometry for long-range H_2-H_2 interaction potential.

$$\frac{3}{\pi}\int_0^\infty \alpha_{\parallel}(i\omega)\,\alpha_{\perp}(i\omega)\,d\omega \quad ,$$

and

$$\frac{3}{\pi}\int_0^\infty \alpha_{\perp}(i\omega)\,\alpha_{\perp}(i\omega)\,d\omega \quad .$$

Upon using the model spectrum, and changing the sign in the denominator of equation (37), trivial calculations yield values of 3.861, 1.232, and 2.426 respectively for $C_{\parallel,\parallel}$, $C_{\perp,\perp}$, and $C_{\parallel,\perp}$, with an expected accuracy of about 1%. Thus,

$$V = -R^{-6}\left\{0.241\left[\sin\theta_a \sin\theta_b \cos(\Phi_a - \Phi_b) - 2\cos\theta_a \cos\theta_b\right]^2 + 3.582\cos^2\theta_a + 3.582\cos^2\theta_b + 9.780\right\} .$$

2. Mars Lander Experiment - Spectral Photometric Day, Twilight, and Night Airglow

In Quarterly Progress Report #1 some discussion was given to the definition of a Mars Lander Experiment designed to perform spectral photometric measurements of the Martian atmospheric day, twilight and night airglows. Some of the required initial tasks were performed in order to make a preliminary evaluation of the feasibility and potential involved in the performance of the experiment.

During the current reporting period this task has been completed. For convenient reference, the results are combined into one detailed report which is given below.

a. Introduction

The identification of both organic and inorganic atomic and molecular constituents in the Martian atmosphere is considered to be fundamental to aeronomic and exobiological studies. In the terrestrial atmospheric case, a most valuable source of these data has been the performance of day, twilight, and night airglow observations employing ground-based spectrophotometric techniques in the visible region of the spectrum. These established techniques can be translated, extended and modified into an appropriate configuration so that similar Martian surface observations may be performed over both the ultraviolet and visible regions of the spectrum.

In Quarterly Progress Report #1 it was demonstrated that airglow experiments can be performed in a more optimum fashion from the Martian surface where many of the constraints for an earth surface platform are minimized. On the basis of the work performed during this quarter, it will be shown that a number of unique opportunities may exist for the generation and subsequent observation of significant signal intensities from solar illuminated constituents in the Martian atmosphere as well as self-emissions due to chemiluminescent reactions and electron and proton bombardment processes involving certain species. Specifically, it can now be demonstrated that the general background radiation applicable to the Martian airglow experiment is about two orders of magnitude less than that encountered on earth and furthermore, that the spectral range of investigation can be extended down to 2000Å. Signal sources involving Martian atmospheric constituents are abundant for the region λλ 2000-3000Å, which is accessible from a Mars-based platform.

A double-pass scanning spectrophotmeter is proposed to scan the region λλ 2000-8000Å; it is a simplified version of a developed capability for use in earth satellites. Since it involves no moving optical

components, it can be packaged for extreme ruggedness in order to survive the relatively high g-loading in the landing environment.

The specific experiments suggested in the following sections involve a host of complex theoretical and practical problems which are considered to lie outside the scope of the present survey and feasibility study. In fact, in some cases, it is difficult to assess the value of performing a specific experiment as compared to other techniques which may be available or have been suggested for the same purpose. Alternatively, it is felt that enough scope and data have been incorporated into the present discussions to amply illustrate the potential involved in a number of applications of airglow observation technology for the identification of specific atomic and molecular constituents in the atmosphere of Mars.

The remaining discussion is presented in the following four sections. The pertinent geometric and solar illumination factors involved in the performance of the proposed Martian twilight, day and night airglow experiments are discussed in Section b, while a number of possible signal generation sources within the spectral range $\lambda\lambda$ 2000-8000Å involving some of the more possible constituents in the Martian atmosphere is included in Section c. For convenience, Section c is divided into five subsections devoted to consideration of the roles of resonance scattering, fluorescence scattering, atmospheric absorption, nightglow, and Martian dust. The experimental configuration of the suggested scanning spectrophotometer is discussed in Section d.

b. On the Geometric and Experimental Configurations Involved in the Performance of Photometric Measurements from a Mars Lander Platform

Most of the pertinent geometric parameters involved in this study are illustrated in Figure 7. In this section, a number of relationships

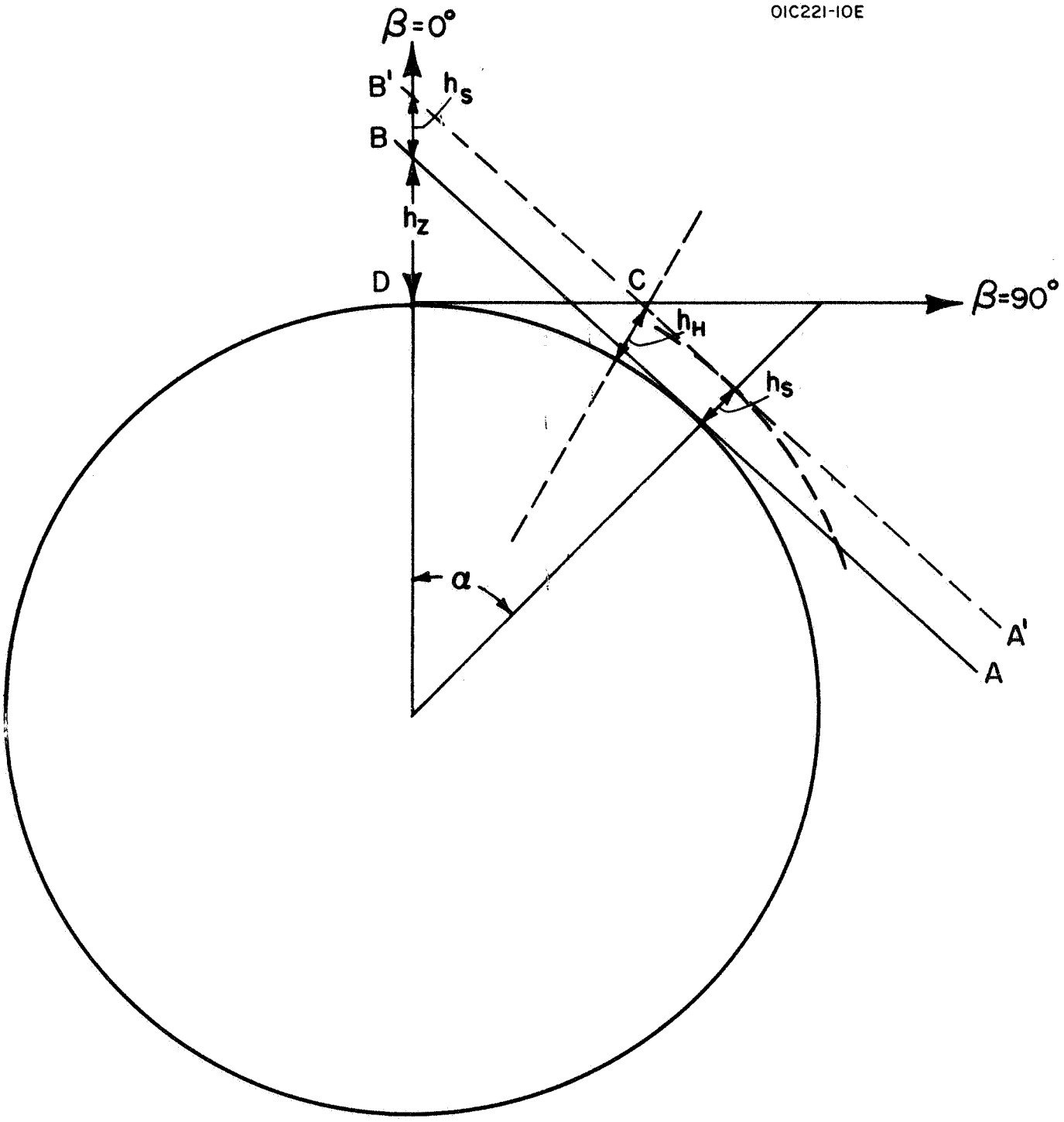

β = Look Angle

h_S = Screening altitude

h_Z = Zenith shadow height

α = Solar depression angle

h_H = Horizon shadow height

Figure 7. Geometry of the Martian airglow spectrophotometric scanning equipment.

will be deduced between these several parameters which are employed subsequently in the development and discussions of the suggested experimental configurations.

Zenith ($\beta = 0^{o}$) sky radiances have been calculated for both earth and Mars for the case of solar zenith angle of zero degrees (i.e., overhead sun) employing available model atmospheres for earth and Mars,[47,48] the appropriate incident solar fluxes[49] and the absorption[50] and Rayleigh scattering[51] characteristics of the several pertinent planetary atmospheric constituents. The results are shown in Figure 8 wherein the heavy dashed and solid curves obtain for the earth and Mars zenith radiances respectively. It should be noted that two separate radiance scales are employed in this figure which illustrates two important factors. First, over the spectral range $\lambda\lambda$ 3000-8000Å, Martian atmospheric background intensities are about two orders of magnitude less than those on earth, (which is roughly equivalent to a platform located at about 30 km above the surface of the earth) and second, the fact that the observational spectral range is extended down to 2000Å for the case of Mars. However, a portion of the apparent improvement in background radiation is due to the scaling factor applied to the lower incident Martian solar flux. Thus, solar flux dependent signal sources would undergo a corresponding decrease whereas in the case of self-emission sources, full advantage can be taken of the lower background radiance conditions. It should be stressed that only the role of Rayleigh scattering has been considered in these calculations so that the presence of a solar-illuminated surface haze layer would result in a Mie scattering background intensity contribution which has not been included herein. In any event, it appears that as far as background considerations are concerned, distinct advantage is obtained with

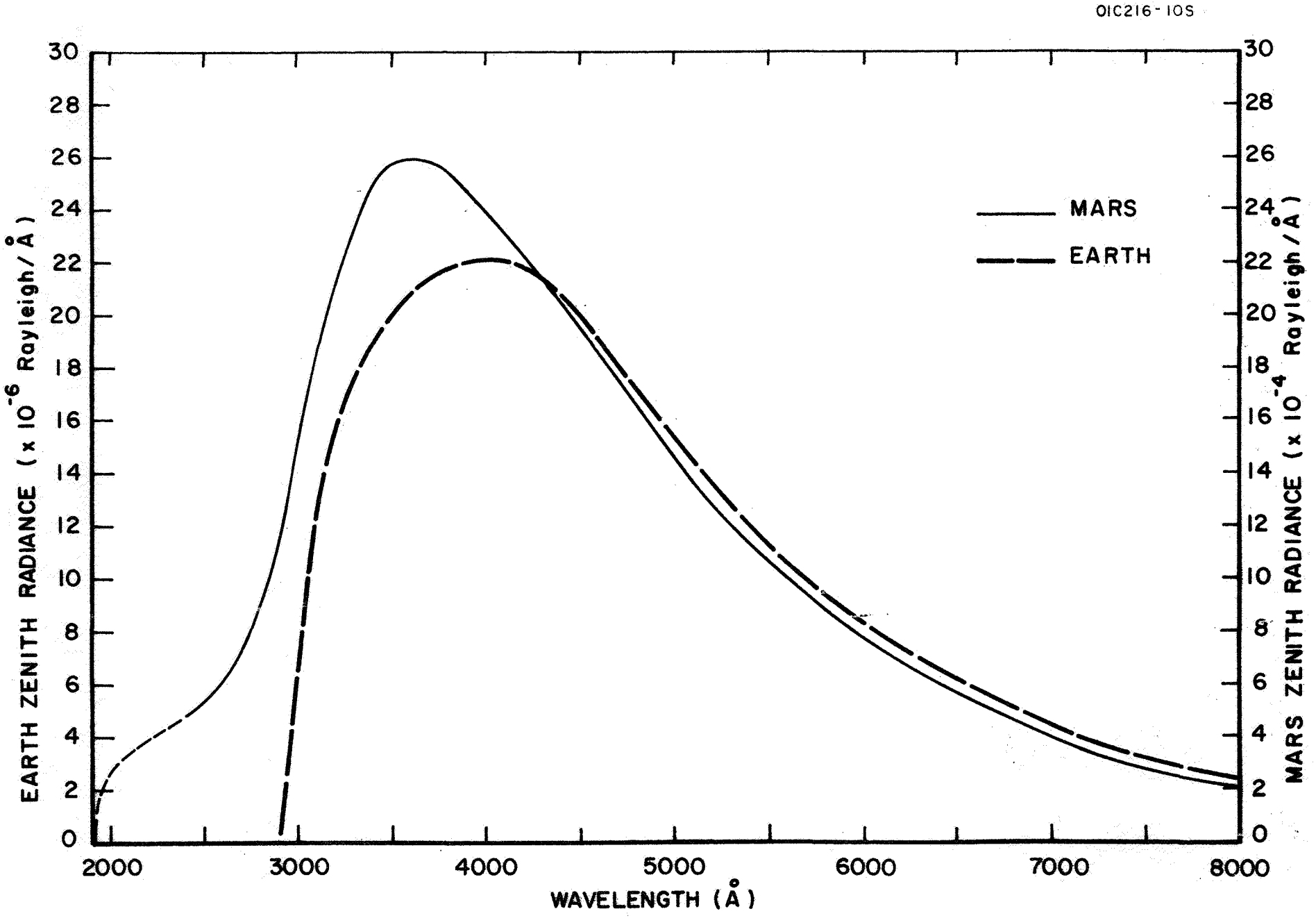

Figure 8. Zenith sky background radiances for Mars and Earth.

respect to the terrestrial atmospheric case for the performance of dayglow observations from the Martian surface.

For the earth case, it has been well established that twilight airglow observations contribute significant data to the aeronomy of the upper atmosphere. In the following discussions, reference is made to the performance of cogent twilight observations in both the zenith ($\beta = 0^{o}$) and horizon (or more appropriately at $\beta \approx 80^{o}$) directions. Accordingly, for subsequent reference it is convenient to derive a number of relationships involving the geometric parameters identified in Figure 7.

The twilight geometry pertinent to planetary atmospheres has been discussed in detail elsewhere.[52] For the simplified case where atmospheric refraction is neglected, a sharp shadow line AB prevails as shown in Figure 7 . Under such conditions, it can be shown that for the zenith look-angle, $\beta = 0^{o}$ and small α-values,

$$h_z \approx \alpha^2 \quad \text{for earth} \tag{44}$$

$$2h_z \approx \alpha^2 \quad \text{for Mars} \tag{45}$$

In addition, for horizon observations performed along $\beta = 90^{o}$, the horizon illumination altitude, h_H as shown in Figure 7 was determined directly from geometric relationships. The zenith and horizon illumination altitudes, h_z and h_H respectively for Mars are shown in Figure 9 in terms of both the solar depression angle, α, in degrees, and in minutes.

Resultant zenith radiances are presented in Figure 10 in terms of Rayleighs/Å as a function of wavelength for $\lambda\lambda$ 2000-8000Å and a number of h_z-values ranging from 0-100 km. For convenience, the corresponding α-values are included on each h_z-curve. The horizon radiance in Rayleighs/Å

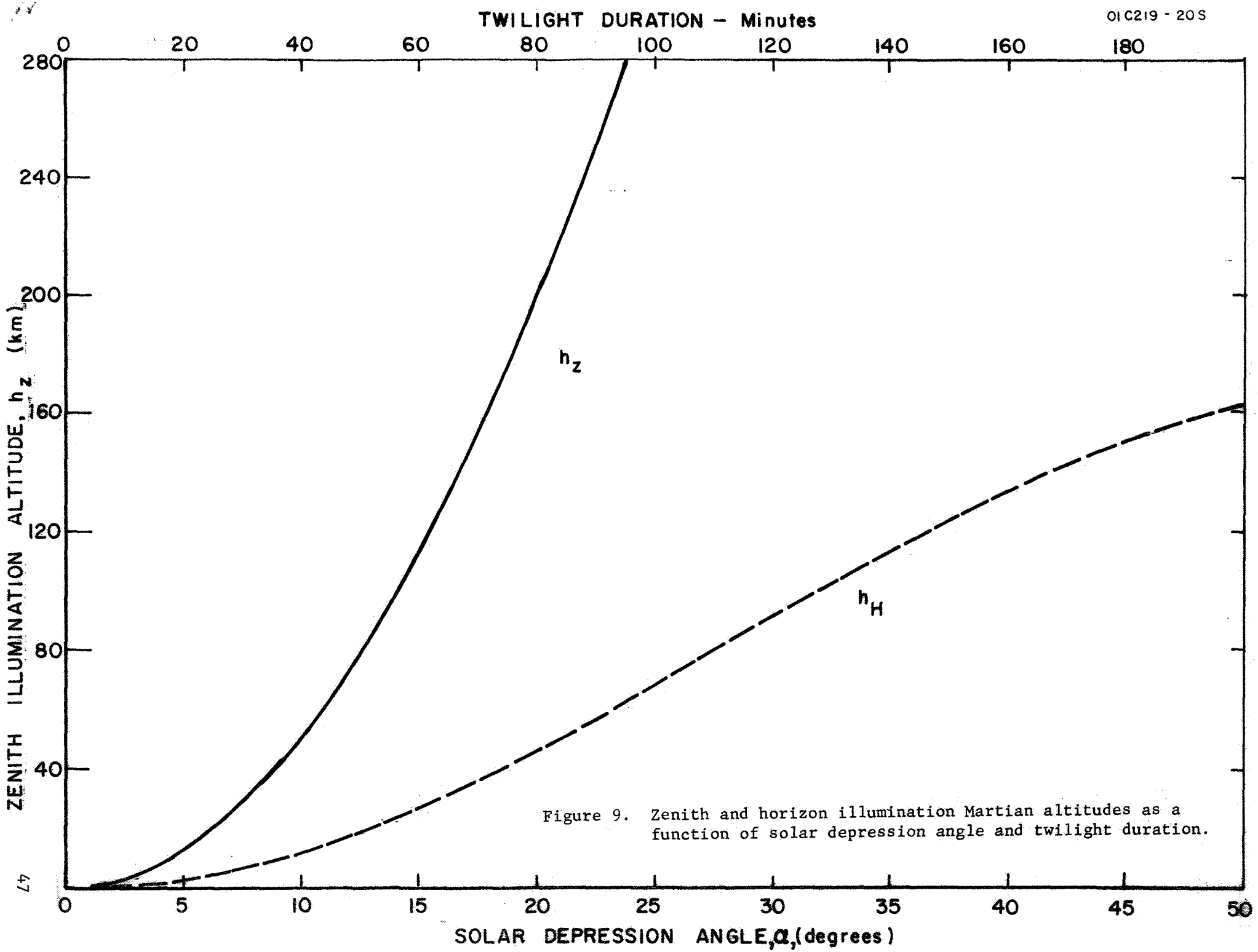

Figure 9. Zenith and horizon illumination Martian altitudes as a function of solar depression angle and twilight duration.

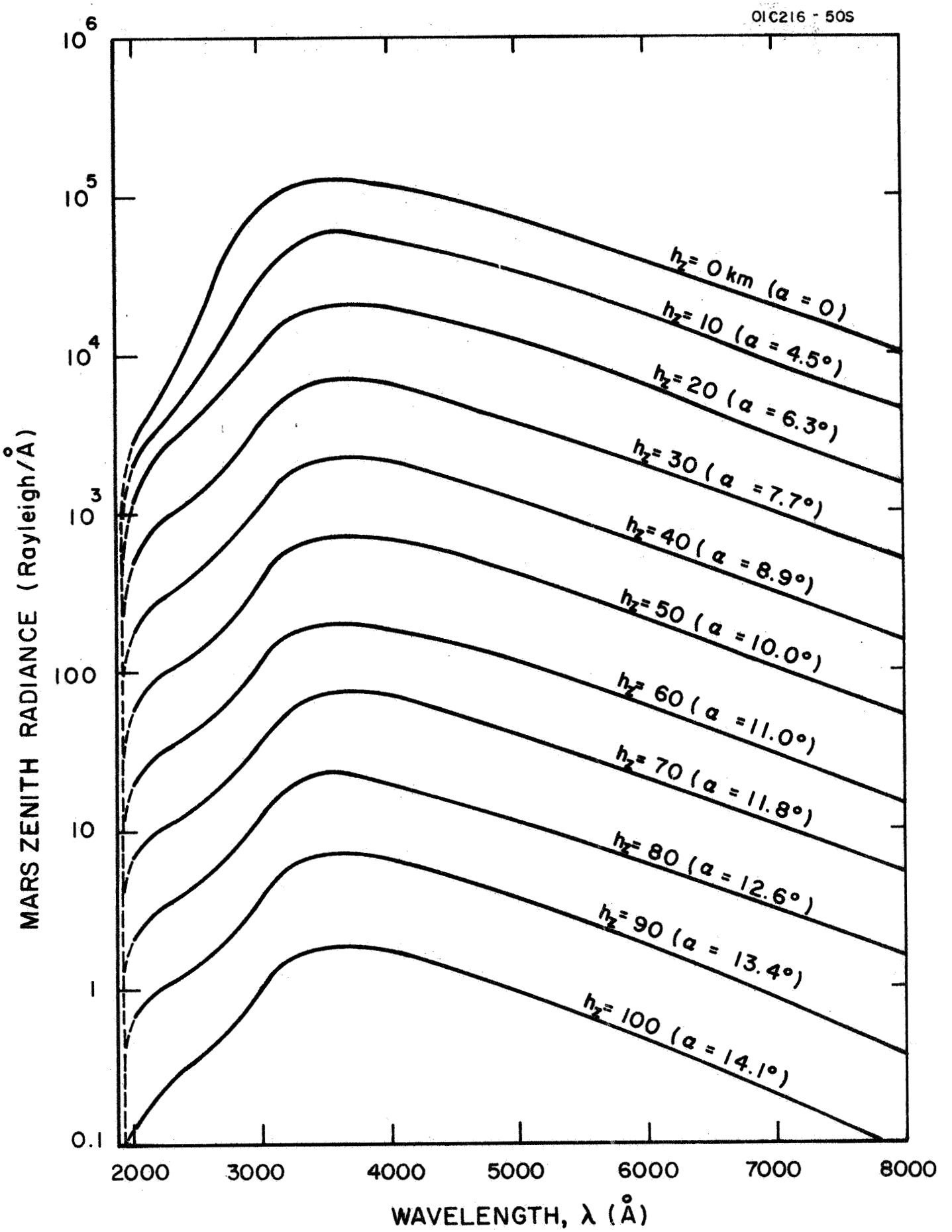

Figure 10. Zenith sky radiance as a function of wavelength for selected solar depression angles.

is presented in Figure 11 as a function of solar depression angle. In this figure, the radiance calculations were performed for three representative wavelengths, namely 2000, 2500, and 3000Å since no significant attenuation occurs for $\lambda\lambda > 3000$Å where the screening height approaches zero km. The screening height, h_s results from attenuation along the twilight path indicated in Figure 7 as A'B'. In the case of Mars, significant attenuation occurs for $\lambda\lambda < 1975$Å where CO_2 absorption predominates. At higher wavelengths, the decreased attenuation is due only to atmospheric Rayleigh scattering by the major constituent model atmosphere gases, i.e., CO_2 and N_2.[48] The sharp increase in h_s-values for $\lambda\lambda < 2000$Å shown in Figure 12 illustrates this point. In the present discussion, the h_s-values are small compared to the radius of the planet at all wavelengths $\lambda\lambda$ 2000-8000Å. Under this condition and for relatively moderate solar depression angles, it is appropriate to simply add the h_s and h_z-values to derive the effective altitude above which resident atmospheric constituents are fully solar illuminated under given twilight conditions. This is illustrated in Figure 7 by the altitude region above the point marked B'.

Estimates were made for the time duration of specific twilight conditions which obtain on both earth and Mars for comparison and reference. For the present purpose, an arbitrary twilight condition is defined for a change in solar depression angle, $\Delta\alpha$ from 1 to 18 degrees (which corresponds to astronomical twilight on earth). The time durations of this condition as a function of date at common latitudes were acquired for both planets. The data, pertinent to the case of earth was deduced directly from data contained in the American Ephemeris and Nautical Almanac. Although corresponding data

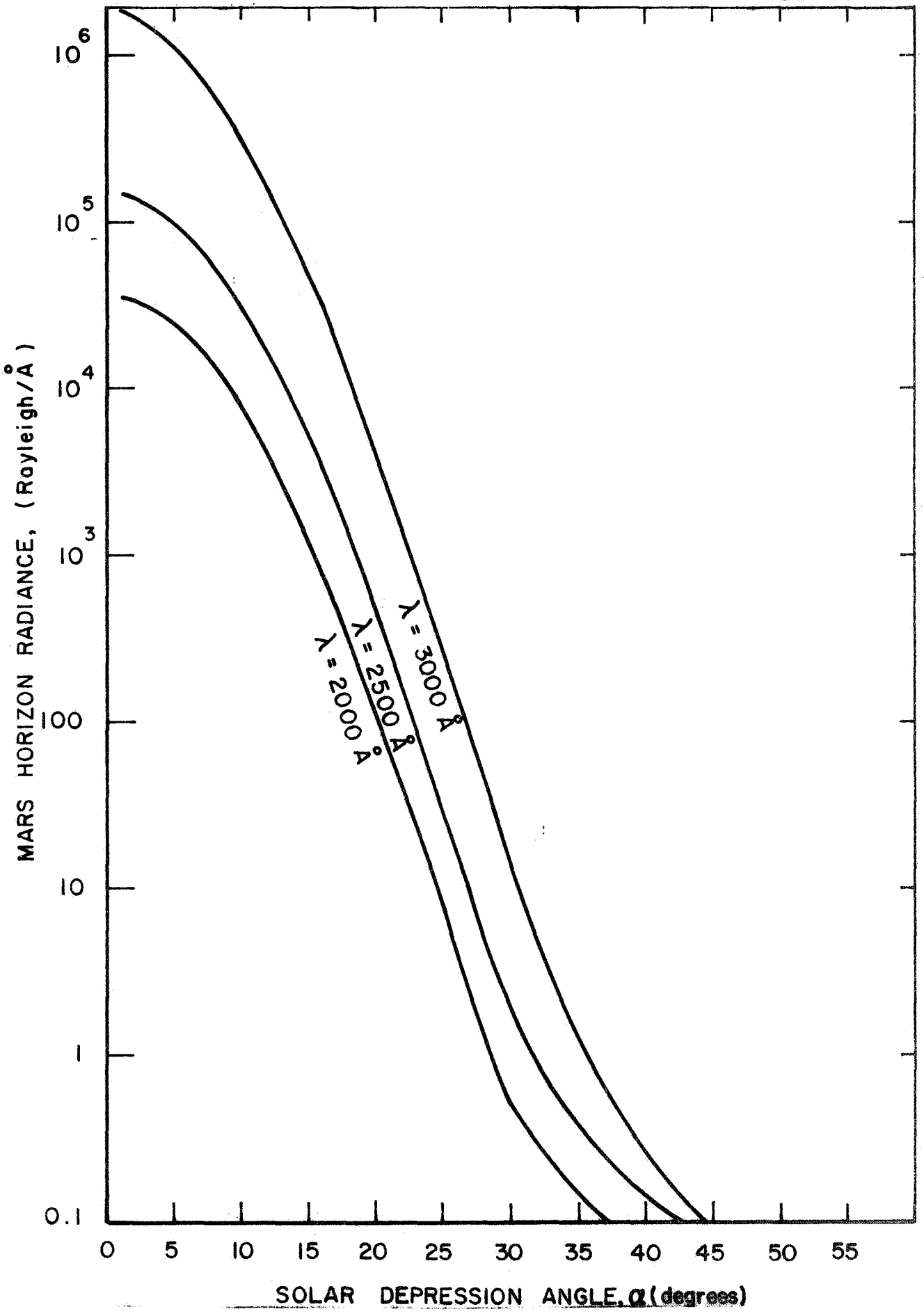

Figure 11. Horizon sky radiance as a function of solar depression angle for λ = 2000, 2500, and 3000Å.

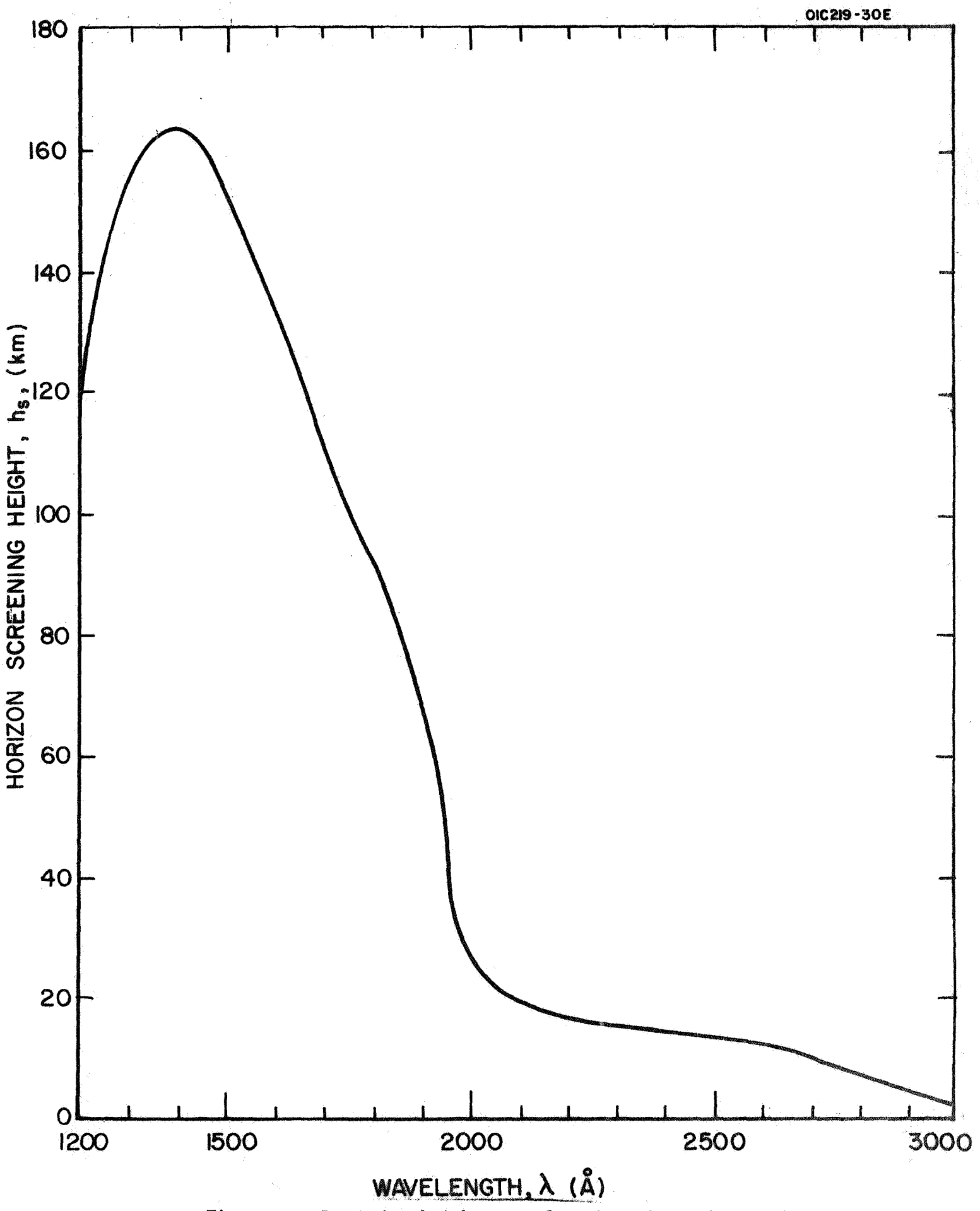

Figure 12. Screening height as a function of wavelength for Martian twilight.

for Mars were not readily available, they were calculated by application of the following expression

$$\Delta t_T = \left| \frac{\tau_o - \tau_T}{360/24.7} \right| \tag{46}$$

Δt_T = time duration for astronomical twilight = $\Delta\alpha$ = 0-18°, cos τ_o = -tan δ tan λ.

$$\cos \tau_T = - \frac{\sin \delta \sin \lambda + \sin \alpha}{\cos \delta \cos \lambda} \tag{47}$$

where δ = solar declination angle

λ = geographic latitude

and α = solar depression angle

The factor 360/24.7 relates to the rotation period pertinent to Mars.

The time duration of astronomical twilight ($\Delta\alpha$ = 0-18°) for the northern hemisphere of earth and Mars are shown in Figures 13 and 14 respectively. The similarity of the Δt_T-values for common latitude is striking although this behavior reflects the ensemble of pertinent planetary and orbital characteristics of the two planets.

In summary then, the following pertinent features can be noted: (a) for the spectral region $\lambda\lambda$ 3000-8000Å, the zenith sky radiance observed on the surface of Mars is about two orders of magnitude less than that which prevails on the earth's surface and that this background corresponds to that encountered from a platform located at a 30 - km earth altitude, (b) for Mars, the spectral region of investigation can be extended down to 2000Å, (c) the time duration of specified twilight conditions for earth and Mars are similar, and (d) for given α-values, the shadow height on Mars is about half of the earth value, which allows increased observation time per

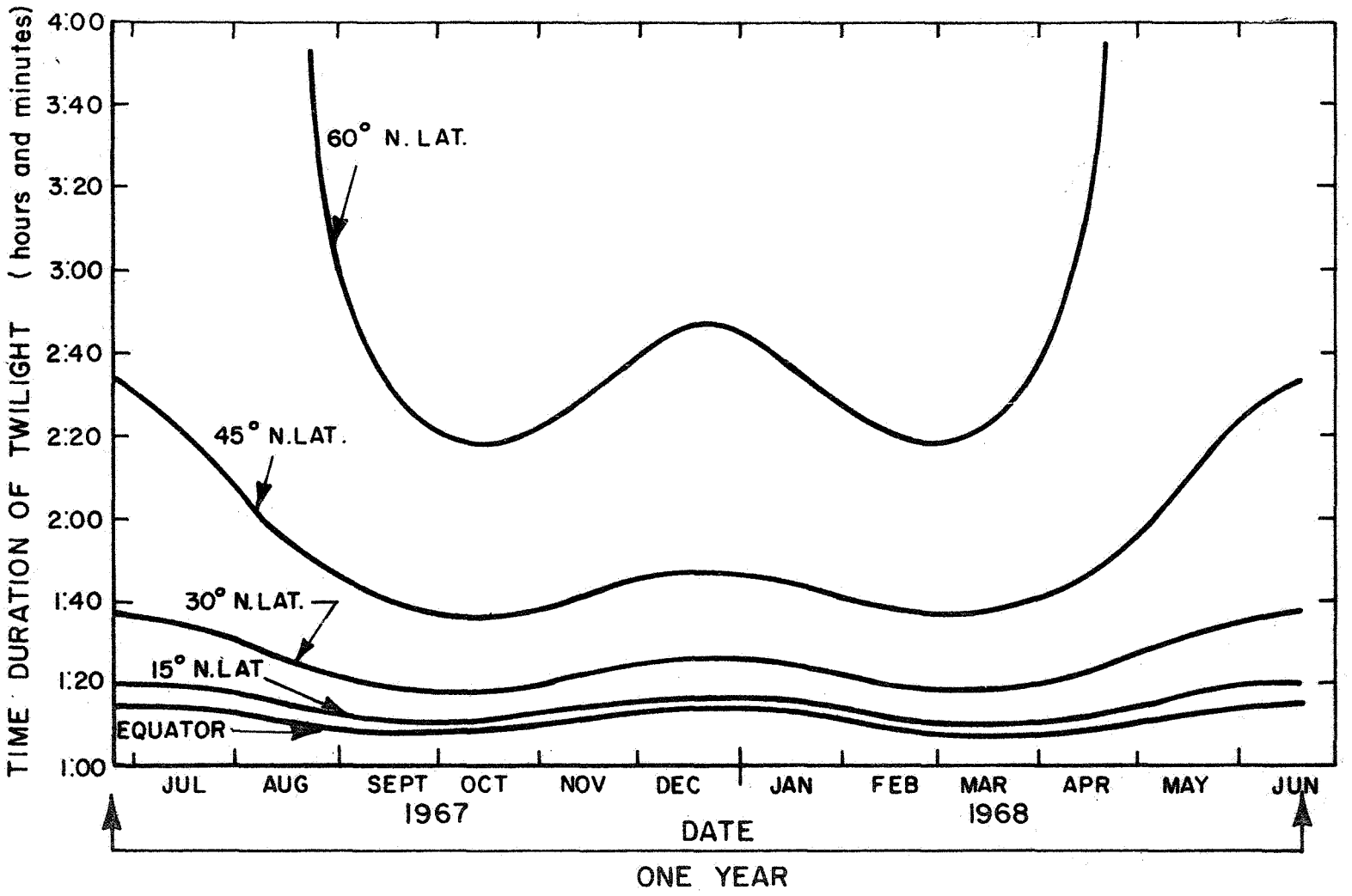

Figure 13. Time duration of twilight for Earth.

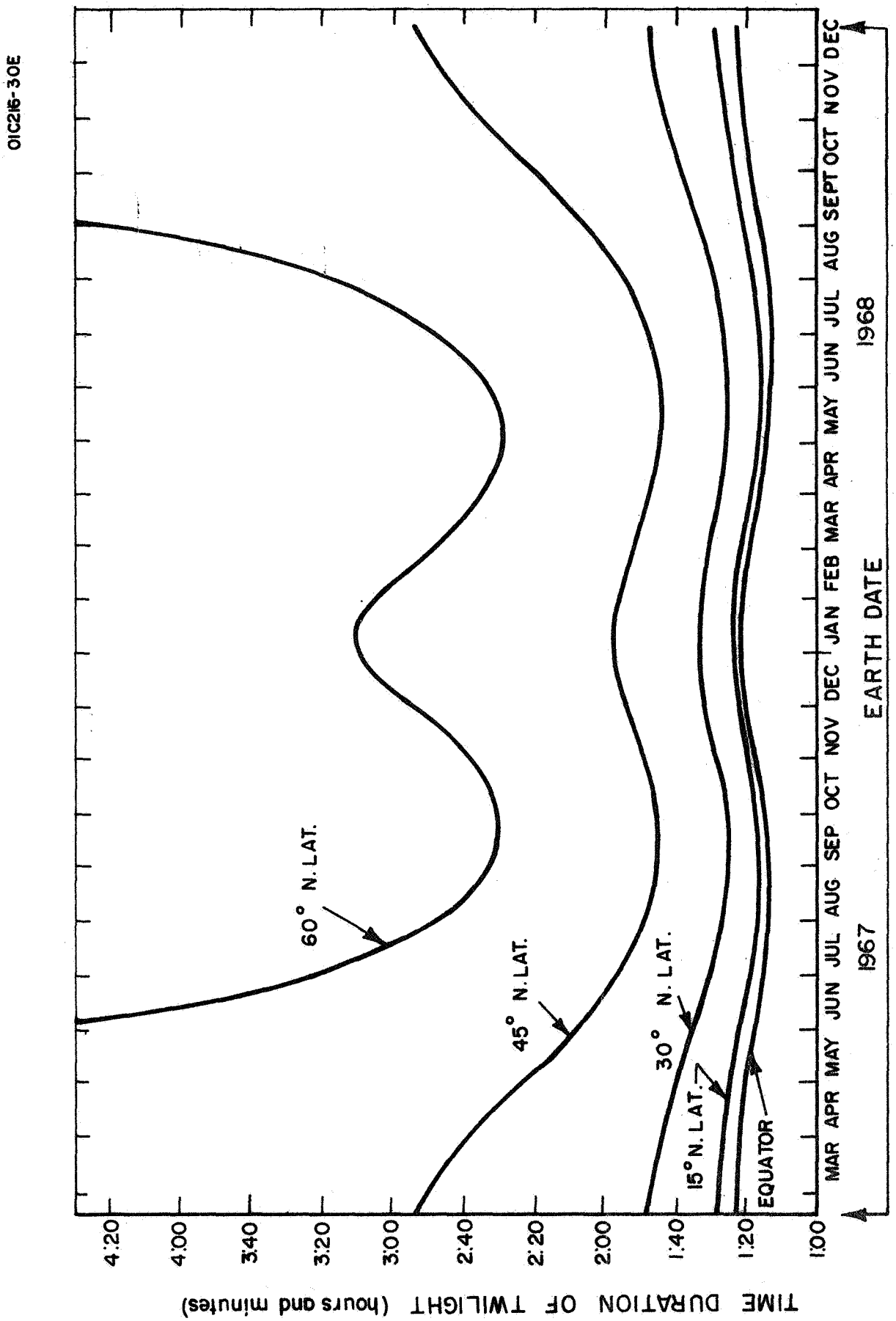

Figure 14. Time duration of twilight for Mars.

unit altitude interval.

The relationships and results presented in Figures 7 through 14 inclusive will be referred to and employed as required in the following discussions which identify a number of possible signal sources which emit throughout the spectral region λλ 2000-8000Å.

c. Potential Signal Sources in the Atmosphere of Mars Owing to the Following Phenomena: Resonance Scattering, Fluorescence Scattering, Chemiluminescence, Absorption, and Particulate Scattering.

In this section, a number of possible signal sources are discussed and evaluated in order to illustrate the potential involved in performing the proposed Martian Lander spectrophotometric experiment. Owing both to the broad scope of the problems encountered and to the required brevity of the presentation, detailed discussions involving parameters which are of necessity somewhat speculative have been avoided. Thus, each signal source category discussed results in the illustration of the potential involved rather than in the recommendation of specific detailed selective experiments. A convenient format has been adopted which incorporates five categories: (1) Resonance Emission from Solar Illuminated Atoms or Ions in the Upper Atmosphere, (2) Fluorescence Emission from Solar Illuminated Molecules or Molecular Ions, (3) Airglow Radiations from Chemiluminescent Reactions between Atmospheric Constituents, (4) Absorption Owing to the Presence of Trace Constituents in the Lower Atmosphere of the Planet, and finally, (5) The Role of Particulate Scattering due to Dust and Haze in the Lower Atmosphere of Mars.

(1) Day and Twilight Airglow Emissions Owing to Resonance Scattering by Solar Illuminated Atoms or Ions in the Upper Atmosphere of Mars

In general, atomic, ionic and metastable species in a planetary atmosphere reside in the upper altitudes owing to recominbation

processes which become more efficient with increasing number densities. The resultant high altitude profiles are particularly amenable to observations conducted under twilight conditions wherein the background radiation can be minimized without significant reduction in the signal intensity. This is not to say that full dayglow observations are precluded; thus for high signal intensity magnitudes, a program of dayglow observations may be warranted.

With certain simplifying assumptions for the case of resonance scattering by atoms or ion species

$$4\pi I = \pi F \frac{\pi e^2}{mc^2} \lambda^2 f\omega \frac{N}{\mu} \tag{48}$$

where $4\pi I$ = the emission rate in photons-cm^{-2}-sec^{-1}-Å^{-1}
(one Rayleigh = 10^6 photons-cm^{-2}-sec^{-1})

πF = the solar flux in photons-cm^{-2}-sec^{-1}-Å^{-1}

λ = resonance wavelength

f = f-value or oscillator strength of the line

ω = the albedo for single scattering

N = number of atoms along the line of sight in atoms-cm^{-2}

μ = cos θ where θ is the angle between the illuminating and observing paths.

For the present purposes, it is convenient to define an emission probability factor, i.e., the number of photons scattered per second per solar illuminated atom:

$$g = \pi F \frac{\pi e^2}{mc^2} \lambda^2 f\omega \tag{49}$$

so that

$$4\pi I = g \frac{N}{\mu} \tag{50}$$

The detailed composition of the Martian atmosphere is unknown at present. However, even with the limited available data, one may speculate that an ensemble of possibilities exist for the production of neutral and metastable atoms and ions in the upper atmosphere. When solar illuminated, these species will re-emit at their characteristic signature resonance radiations which can represent possible signal sources of interest for λλ 2000-8000Å. Among the generation processes are included: ionospheric recombination, solar photodissociation, photoelectron and solar wind proton interaction with the atmospheric constituents, photochemical production of these species, etc. Under certain conditions, it can be expected that the resultant resonance signals could be highly intense. For example, in the terrestrial atmosphere case, the $[OI]_{21}$-6300Å and the sodium-D-5890Å radiations (on the order of 20kR) have been observed in full dayglow experiments by Noxon and Goody[53] and Donahue[54] respectively, in spite of the intense earth background radiations shown in Figure 8 at these spectral positions. Since the corresponding background intensities pertinent to Mars are two orders of magnitude lower, it is evident that in the proposed Martian surface experiment similar and lesser emission intensities could be observed in the dayglow. Another possible source of atmospheric atoms and ions results from the deposition and subsequent observation of interplanetary debris in the upper atmosphere of Mars. This latter source is singled out for more detailed discussion in order to illustrate the potential involved.

Interplanetary debris represents an important source of minor constituent atoms and ions in the upper atmosphere of the earth. The identity and inventory of these debris atoms and ions have been experimentally confirmed for Na^+, Mg^+, $A\ell^+$, Ca^+, Fe^+ and Si^+[55] by direct in-situ measurements and also for Ca^+, Na, K and Li[56] by ground-based photometric twilight

observations. The observed atomic number density-altitude profiles typically peak in the vicinity of 100 km with a sharp cutoff occurring at lower altitudes due to the occurrence of oxidation processes. It may be speculated that a somewhat similar situation obtains in the upper atmosphere of Mars. In fact, on the basis of an analysis performed by Marmo and Brown,[57] it has been shown that assuming equivalent debris influx rates, for the case of Mars the peak number density would be larger (due to the limited oxidation processes compared to earth) and also it would occur at altitudes in the vicinity of 80 km. In any case, it appears reasonable to search for the presence of these debris species in the upper atmosphere of Mars. To emphasize this possibility, the following preliminary analysis was performed.

First, a number of possible debris constituents were selected on the basis of two criteria: (a) that they possess a relatively high chemical abundance in typical meteors,[58] and (b) that their resonance wavelengths are located at $\lambda\lambda > 2000$Å.[59] The selected debris atoms and their corresponding resonance wavelengths are presented in columns 1 and 2, respectively of Table V. From readily available data[59,60] corresponding g-values were calculated as shown in column 3 of Table V. Relative signal intensity estimates can be derived for the tabulated species as follows. First, it is assumed that the deposited inventory of the upper atmospheric debris species is equivalent to its chemical abundances in typical meteors. Then if C represents this abundance parameter, the product gC-values in column 4 of Table V are measures of the expected relative signal intensities. It is convenient to normalize these values to sodium which is assigned an arbitrary value of unity. As noted previously, a representative earth value for the Na-D-5890Å dayglow

TABLE V

Relative Emission Probability - Abundance Factors (gC-values), for Solar Illuminated Meteoric Debris Atomic and/or Ionic Species in the Martian Atmosphere

Debris Species	Resonance Wavelength Å	$g\left(\frac{\text{photon}}{\text{sec-atom}}\right)^{*}$	gC-values**
Aℓ I	3082	7.6(-2)	2.6(-1)
Ca I	4227	1.0(-2)	1.7(-2)
Ca II	3933	1.4(-1)	
Fe I	3441	7.6(-3)	6.0(-1)
Fe II	2599	2.2(-2)	
K I	7699	1.2(-1)	1.4(-1)
Li I	6708	4.4(0)	1.6(-2)
Mg I	2852	1.0(-1)	3.2(0)
Mg II	2796	3.1(-2)	
Na I	5890	6.4(-1)	1.0(0)
Ni I	3370	8.2(-2)	7.9(-2)
Si I	2514	6.0(-3)	2.1(-1)
Ti I	3342	4.0(-2)	3.4(-2)

* Values in parenthesis are raised to that power of ten

** gC-values are relative to a value of unity for sodium

can be taken as about 20 kR.[52] If this signal intensity value is employed as a reasonable estimate for the Mars dayglow, it follows that all the species indicated in Table V should be readily observable under certain specified conditions (of both dayglow and twilight airglow) encountered during the conduct of the suggested experimental program.

(2) Day and Twilight Airglow Emissions Owing to Fluorescence Scattering by Solar Illuminated Molecules and Molecular Ions in the Atmosphere of Mars

Molecules and molecular ions which may represent sources of Martian atmospheric emission included the following candidates: CO, NO, O_2, N_2, OH, CN, N_2^+, O_2^+, CO^+, CO_2^+, and others. Therefore, the resultant fluorescence over the spectral region of interest $\lambda\lambda$ 2000-8000Å owing to the initial absorption of solar radiation by these molecules constitutes another signal source which is evaluated in the following discussion.

The molecular case is more complex than its atomic analog discussed previously although the single scattering theory for atoms may be adapted readily for application to diatomic molecules. The expression which describes single molecular photon scattering is analogous to Equation (48) for atomic species and is given by:

$$4\pi I_{v'v''} = \pi F_{v'o} \frac{\pi e^2}{mc^2} \lambda^2_{v'o} f_{v'o} \omega_{v'v''} \frac{N_o}{\mu} \qquad (51)$$

where the v'v'' subscripts emphasize the fact that the initial absorption may occur in one electronic-vibrational transition while the subsequent fluorescence may occur at longer wavelengths involving other electronic-vibrational transitions. In the above expression, the F, f, and λ-values have subscripts v'o to indicate involvement of the absorption band of the lowest vibrational level (v'' = 0) of the ground electronic state. The N_o-value indicates that the

participating molecules generally reside at the lowest vibrational level of the ground state. As a further analogy to the case of atoms, the emission probability factor for molecular fluorescence may be expressed as

$$g_{v'v''} = \pi F_{v'o} \frac{\pi e^2}{mc^2} \lambda^2_{v'o} f_{v'o} \omega_{v'v''} \tag{52}$$

so that

$$4\pi I_{v'v''} = g_{v'v''} \frac{N_o}{\mu} \tag{53}$$

In general, the pertinent molecular f-values are not available so that the corresponding $g_{v'v''}$-factors are not readily calculable. However, the relative intensity distribution of the molecular resonance and fluorescent bands can be deduced for an optically thick atmosphere on the basis of the published theoretical results of Chamberlain and Sobouti.[61] They have shown that for this case

$$4\pi I_{v'v''} = \pi F_{v'o} \omega_{v'v''} \Delta\lambda \frac{\mu_o}{\mu} H(\mu_o) \tag{54}$$

where $H(\mu_o)$ are tabulated functions by Chandrasekhar[62] and $\Delta\lambda$ is the effective line-width.[61] Thus, the relative intensities of both the resonance and fluorescence bands are proportional to the solar flux, $F_{v'o}$ and the albedo for single scattering, $\omega_{v'v''}$. The $f_{v'o}$-values are not involved in Equation (54) since the solar flux penetrates into the optically thick atmosphere to saturate the bands. If the $\Delta\lambda(\mu_o/\mu)H$-value is assigned the value of unity, then

$$4\pi I_{v'v''} \approx \pi F_{v'o} \omega_{v'v''} \tag{55}$$

which yields reasonable signal estimates for the optically thick case, as well as indicating the relative intensities in a given fully solar illuminated band system.

A number of pertinent parameters for several possible molecular constituents in the Martian atmosphere are summarized in Table VI. The band systems are identified and the appropriate electronic transitions are indicated in column 2 while column 3 includes some selected v'-v" transitions and their corresponding λ-values as presented by Barth.[63] In each case, the initial absorption (i.e., v'o) transition can be identified easily while the subsequent fluorescent emissions were selected on the basis of their relative efficiency over the spectral region $\lambda\lambda > 2000\text{Å}$. In accordance with Equation (55), the $4\pi F_{v'o}\ \omega_{v'v''}$-values corresponding to the selected fluorescent emission bands are presented in column 4 of the table. At best, these values represent maximum signal estimates which can be expected to be reduced significantly in practice for specific cases. Finally, some general comments are presented in column 6 which are pertinent to each of the individual transitions.

Detailed evaluation of the probability of observing any specific emission indicated in the table would require a complex analysis where much of the basic input data which at this point are at best speculative or just not avilable. For example, it is important to ascertain whether a particular molecular constituent is well-mixed or is resident in layer form in the upper Martian atmosphere. It can be assumed that the major model atmospheric constituents, N_2 and CO_2 are mixed, while for such species as OH, CN, N_2^+, O_2^+, CO^+, and CO_2^+ layering could be invoked. Furthermore, for such molecules as CO, NO, and O_2 the atmospheric distribution question can not be answered at this time. Additionally, an important factor in evaluation of twilight observation of molecular fluorescence involves the horizon screening height shown in Figure 12 and discussed in Section b. For example, if the initial

TABLE VI

Molecular Constituent	Band System Transition	Absorption-Fluorescence Transition v'-v''	λ	$F_{v'o}\omega$ - value, photons/cm^2/sec/Å	Comments
CO	4^{th} Pos. System $A\ ^1\Pi - X\ ^1\Sigma^+$	5-0	1393	2.8 (7)	Allowed Transition Screening height for 1393Å ≈ 160km (see Fig.)
		5-11	2012	1.5 (7)	
		5-12	2089	1.8 (7)	
		5-13	2172	1.1 (7)	
	Hopfield-Birge Bands $a'\ ^3\Sigma^+ - X'\ ^1\Sigma^+$	0-0	1804	2.9 (6)	Forbidden Transition Screening height for 1804Å ≈ 90km
		0-5	2223	1.1 (9)	
		0-6	2327	1.3 (9)	
		0-7	2440	1.3 (9)	
	Cameron Bands $a\ ^2\Pi - X\ ^1\Sigma^+$	0-0	2063	2.3 (10)	Forbidden Transition Screening height for 2063Å ≈ 20km Very rich fluorescence spectrum for λλ 2000-2800Å (a)
		0-1	2158	2.8 (10)	
NO	Gamma Bands $^2\Sigma^+ - X\ ^2\Pi$	0-0	2262	5.9 (10)	Allowed Transition Screening height for 2262Å ≈ 15km Screening height for 2149Å ≈ 15km
		0-1	2363	8.2 (10)	
		1-0	2149	9.8 (10)	
O_2	Schumann-Runge $B\ ^3\Sigma_u^- - X\ ^3\Sigma_g^-$	0-0	2026	8.0 (2)	Allowed Transition Screening height for 2026Å ≈ 20km Fluorescence spectrum rich in bands for λλ 1700Å - 4000Å (b)
		0-12	3105	8.0 (9)	
		0-13	3234	8.8 (9)	
	Herzberg Bands $A\ ^2\Sigma_u - X\ ^3\Sigma_g^-$	0-0	2885	2.4 (7)	Forbidden Transition Screening height for 2885Å ≈ 5km Fluorescence spectrum rich in bands for λλ 2400-5000Å (c)
		0-8	4370	3.8 (11)	
		0-9	4647	3.9 (11)	
		0-10	4955	3.2 (11)	

Molecular Constituent	Band System Transition	Absorption-Fluorescence Transition $v'-v''$	λ	$F_{v'o}\omega$ - value photons/cm^2/sec/Å	Comments
N_2	Vegard-Kaplan Bands $A\ ^2\Sigma_u^+ - X\ ^1\Sigma_g^+$	0-0	2010	7.8 (7)	Forbidden Transition Screening height for 2010Å ≈ 20km
		0-4	2463	8.5 (9)	
		0-5	2605	1.0 (10)	
		0-6	2762	9.7 (9)	
	Hopfield-Birge Bands $b\ ^1\Pi_u - X\ ^1\Sigma_g^+$	0-0	986		Allowed transition Screening height for 986Å > 200km No significant fluorescence for λ > 2000Å
	Lyman-Birge-Hopfield Bands $a\ \Pi_g - X\ ^1\Sigma_g$	0-0	1450	1.5 (7)	Forbidden transition Screening height for 1450Å ≈ 150km Photon emission flux for λ > 2000Å too weak to observe
		0-9	2040	5.0 (4)	
		0-10	2130	7.1 (3)	
		0-11	2227	7.3 (2)	
OH	Hydroxyl UV Bands $A\ ^2\Sigma^+ - X\ ^2\Pi$	0-0	3064	4.0 (12)	Allowed transition The g-values for the transitions 0-0, and 1-0 are 8.6 (-4) and 2.4 (-5) photon-sec-atom respectively (d)
		1-0	2811	5.4 (11)	
CN	Cyanogen Violet Bands $B\ ^2\Sigma^+ - X\ ^2\Sigma^+$	0-0	3876	8.1 (12)	Allowed transition The g-values for the transitions 0-0, and 1-0 are 7.4 (-2) and 7.3 (-4) photon-sec-atom respectively (e)
		1-0	3582	9.2 (11)	
N_2^+	First Negative Bands $B\ ^2\Sigma_u^+ - X\ ^2\Sigma_g^+$	0-0	3914	6.4 (12)	Allowed transition From published f-values, 4 x 10^{10} ion-cm^2 results in signal intensity of 1 kR.

Molecular Constituent	Band System Transition	Absorption-Fluorescence Transition v'v''	λ	$F_{v'o}\omega$ - value photons/cm^2/sec/Å	Comments
O_2^+	Second Negative System $A\ ^2\Pi_u - X\ ^2\Pi_g$	0-0 11-0 11-1	2610 2153 2242	8.0 (6) 2.0 (10) 6.0 (10)	Allowed transition Screening height for 2610 ≈ 15km
CO^+	First Negative Band $B\ ^2\Sigma^+ - X\ ^2\Sigma^+$	0-0	2191	1.4 (11)	Allowed transition Screening height for 2191Å ≈ 15km The g-value for the transition 0-0 is 1.2×10^{-4} photons-sec-atom (f)
	Comet Tail Bands $A\ ^2\Pi - X\ ^2\Sigma^+$	0-0 0-1	4900 5487	2.2 (12) 5.5 (12)	Allowed transition The g-value for the transition 2-0 is 1.3×10^{-3} photon-sec-atom (g)
CO_2^+	Fox, Duffendale and Barker Comet Bands $^2\Pi_u - X\ ^2\Pi_g$		3378 3505 3674	5.0 (11)* 5.0 (11) 5.0 (11)	Allowed transition Intense bands seen in comets by fluorescence radiation. (h) Believed to be initially excited by λ ≈ 2800Å; screening height ≈ 5km.

(a) Barth, C. A., UV Spectroscopy of Planets, JPL TR No. 32-822 (December 15, 1965)(see Figure 20)
(b) Ibid, see Figure 5
(c) Ibid, see Figure 8
(d) Ibid, see Table X
(e) Ibid, see Table XI
(f) Lawrence, G. M., Journal of Quantitative Spectroscopy and Radiative Transfer, 5, No. 2, 359 (1965)
(g) Dalby, F. W., Handbuch der Physik, 27, 464 (1964)
(h) Dufay, M. and Poulizac, M. C., Memoires de La Societe Royales de Sciences de Liege, pp. 427 (c.1966)

absorption occurs at a wavelength of about 1400Å, (i.e., see the 4th positive 5-0 transition for CO in Table VI) the resultant screening height is approximately 160 km. When this value is added to the h_z-values of Figure 10 , it is evident that the column count of solar-illuminated CO molecules is relatively limited. Accordingly, under certain conditions it may be advantageous to select absorption transitions which involve relatively long wavelengths and correspondingly lower screening heights. Additionally, it should be noted that unless the molecular constituent resides in an atmospheric layer configuration, the performance of twilight measurements may not be particularly advantageous. Alternatively, the performance of both day and twilight airglow experiments could provide data from which the existence of either the mixing or layering configuration could be ascertained. Finally, the role of quenching must be considered for relatively low altitude airglow phenomena. This is expecially true in cases where forbidden transitions (i.e., long lifetimes) are involved.

Many of the transitions specified in Table VI can result in fluorescence caused by the interaction of photoelectrons in the upper atmosphere of Mars. It should be noted that in the earth case for certain constituents, this phenomena represents the major emission factor so that its effect on Mars should also be recognized. However, this well known additive source function is not stressed here since it is a tractable problem so long as the appropriate data are available.

On the basis of the foregoing discussions, and the data presented in Table VI , it is evident that the definition of specific measurements is an extremely complex matter. However, with appropriate effort, some

selectivity for the ensemble of possibilities in Table VI could be made in order to isolate the more promising cases. For the present purposes, this task is considered to lie beyond the scope of this presentation.

In summary, then, it is felt that the data shown in Table VI and the foregoing discussions indicate the potential of performing fluorescence experiments in the spectral region $\lambda\lambda > 2000$Å, in order to identify a number of possibly important molecular constituents in the Martian atmosphere and ionosphere.

(3) Twilight and Night Airglow Emissions from Chemiluminescence Processes Occurring in the Upper Atmosphere of Mars

It is conjectured that various possibilities exist for the generation of chemiluminescent atomic and molecular emissions due to reactions between ambient chemical constituents in the Martian atmosphere. As an example of the former, (atomic emissions) chemiluminescence may result typically from the debris species enumerated in Table V by mechanisms related to those which photochemically produce the nighttime sodium-D lines observed in the earth's atmosphere. In addition, twilight and night airglow emissions at 6300, 6364, 5199Å, etc. may be produced from a variety of processes which include photodissociation, recombination, photoionization, electron and proton impact, etc. Concerning molecular system chemiluminescence, it has been suggested that a significant portion of the terrestrial night airglow is attributable to the production of NO_2^* produced by the reaction between NO and O. This process as well as a similar one involving CO and O may occur in the Martian atmosphere. These latter two possibilities are discussed in a more

detailed evaluation below where resultant order of magnitude signal intensity estimates are derived.

Inn[64] first suggested that the blue haze observed on Mars may be due to chemiluminescence from a reaction involving CO and O which resulted in the production of excited CO_2^*. The subsequent emission from this excited species resides in a band system in the spectral region λλ 3200-6000Å with a peak intensity occurring at a wavelength of 4000Å. The spectrum was photographed and classified by Mahan and Solo[65] who reported that this system consisted of 250 bands with relatively little continuum background. Inn[64] employed a photochemical equilibrium model (using local number densities for $[CO] = [O] = 10^{12}$ cm^{-3} at an altitude of about 100 km) and the chemiluminescence efficiency data of Clyne and Thrush[66] to estimate a total band system brightness of about 20 kR. On the basis of this value and the spectral distribution observed by Mahan and Solo,[65] it can be estimated that the signal brightness of the most intense band of the system could amount to about 1 kR. A signal intensity of this magnitude would be easily detectable under the appropriate twilight conditions (see Figures 10 and 11).

With respect to the possibility of observing the NO_2^* emissions in the twilight or night airglow, it is necessary to establish an upper limit value for NO in the Martian atmosphere. Marmo and Warneck[67] have shown recently that under thermodynamic equilibrium an NO/O_2 ratio > 1 obtains throughout the mixed region of the Martian Atmosphere. Additionally, Belton and Hunten[68] experimentally established an upper limit value for O_2 of about 20 cm-atm. or about 5.4×10^{20} cm^2 column in the Martian atmosphere.

If this value is also applied to the case of NO, then in a mixed atmosphere, at an altitude of about 100 km the local number density of NO, $[NO] \approx 10^{11} cm^{-3}$. Jonathan and Doherty[69] have demonstrated that the chemiluminescence efficiency for the NO_2^* emissions is about 2000 times greater than that measured for the CO_2^* throughout the investigated spectral ranges. Thus, it is evident that under conditions similar to those specified by Inn[64] (i.e., where $[O] = 10^{12}$ cm^{-3}) the resultant chemiluminescent signal intensity may be as large as 4×10^3 kR. However, it should be noted that this latter value is predicated on the photon emission rate over the entire continuum which extends over a spectral interval of about 2000Å. Thus, on a unit spectral interval basis, the average chemiluminescence signal amounts to about 2 kR/Å. However, since the continuum peaks around 6200Å, observations conducted at this spectral position can be expected to amount to about an order of magnitude greater or about 20 kR/Å. Clearly, such signal magnitudes could be observed easily during the course of the proposed experiment. However, in reality the local NO number density at a Martian atmosphere altitude of 100 km is probably less than 10^{11} cm^{-3} so that a concommitant reduction in signal intensities would result.

Finally, with respect to the two chemiluminescent reaction examples discussed above, it should be noted that the pertinent chemical consumption rates are such that the active constituent number densities are essentially conserved throughout the night. Under these minimum background intensity conditions, it is evident that a sensitive technique is available for positively observing and identifying these emissions and subsequently establishing meaningful upper limit values for the constituents involved.

(4) The Detection, Identification, and Measurement of Altitude Profiles of Minor Constituents in the Lower Atmosphere of Mars

In this section is described an experimental technique designed to detect, identify, and measure the altitude profiles of minor constituent absorbing species in the lower atmosphere of Mars. For this purpose, twilight measurements are performed to measure the irradiances of both the zenith and horizon directions. It will be demonstrated that these irradiances are sensitively perturbed by the presence of absorbing trace constituents in the lower atmosphere of Mars. This technique involves the following advantages: (a) the detection capability is enhanced by about a factor of 25 greater than that available with currently employed techniques; (b) the unambiguous identification of the constituent involved is possible owing to its absorbing characteristic for $\lambda\lambda > 2000\text{Å}$; and finally (c) the species altitude distribution can be ascertained on the basis of the geometric factors involved in the performance of cogent twilight experiments.

As discussed previously, the Martian atmosphere is essentially transparent to solar zenith radiation for wavelengths above about 2000Å as shown by the results of Figure 8 and confirmed by the recent observations of Evans.[70] On this basis, it is possible to experimentally establish upper limit vertical column count values for any gas which absorbs radiations of wavelengths greater than 2000Å. For example, employing the measured absorption cross-sections for ozone in this spectral region,[50] a corresponding upper limit vertical count value of about 1×10^{17} cm^2 column can be established. Identification of the existence and establishment of the upper limit estimate

of the content of this particular constituent has important implications on both aeronomic and biological processes occurring in the Martian atmosphere.

Similarly, upper limit values can be established for other potentially important species which exhibit distinctive absorption features. The absorption curves for a number of such potentially important candidate species which qualify in this regard are presented in Figures 15, 16, and 17 over the spectral region λλ 2000-3000Å. These data were extracted directly from Calvert and Pitts.[71] It should be noted that the curves pertinent to inorganic species are presented in Figure 15 while the absorption characteristics of several interesting organic materials, which may be related to biological interests, are shown in Figures 16 and 17.

With respect to the data of Figure 15, it should be noted that in biological processes, H_2O_2 is required to oxidize both sulfides and certain carbon compounds to simple sulfates and carbonates. In addition, Marmo and Warneck[67] have demonstrated that SO_2 or H_2S can participate as precursor sources for sulfur in the photochemical generation of sulfur containing amino acids in the Martian atmosphere. Marmo and Warneck[67] have also shown that, in the Martian atmosphere, a thermodynamic relationship obtains for the NO/O_2 ratio, which can be further related to the content of NO_2, N_2O, and NOCℓ so that the presence of these constituents may involve both important aeronomic and biological implications. For inorganic gases, a number of additional candidate species have been enumerated previously in Table VI where appropriate absorption ($v'' = 0$) bands are shown to occur at $\lambda > 2000$Å for several transitions.

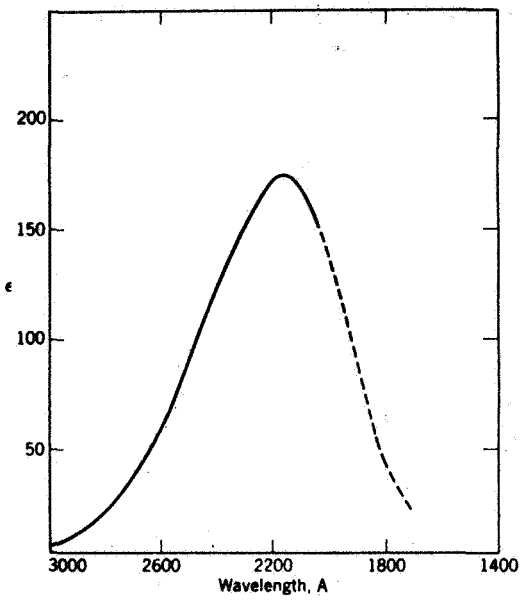

Absorption spectrum of HI. From Romand.

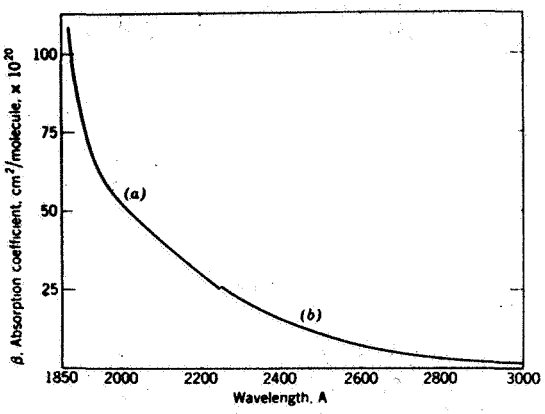

The absorption spectrum of H_2O_2 vapor; the absorption coefficient β is defined by $\beta = 2.303 \log (I_0/I)/nl$, where n is the concentration in molecules/cubic centimeter and l the path in centimeters. From Volman,[54] originally from Refs. 55 (curve *a*) and 56 (curve *b*).

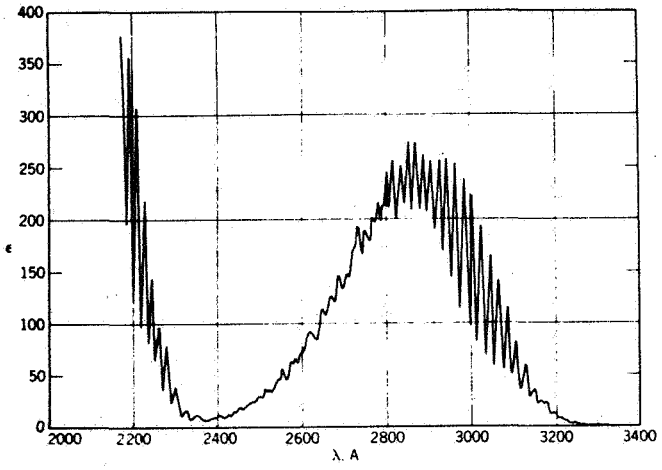

The absorption spectrum of $SO_2(g)$. 25 . Spectra determined by Mrs. Veronique McMillan

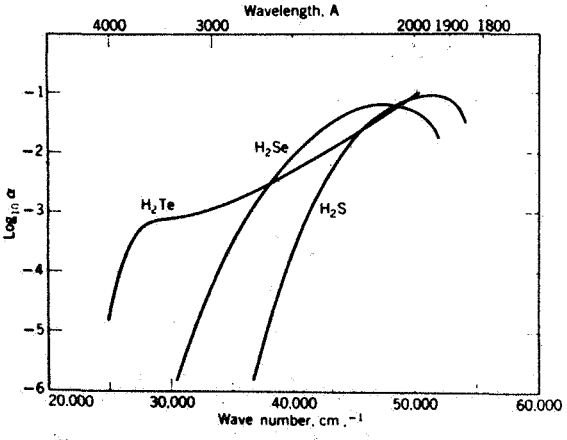

The absorption spectrum of H_2S, H_2Se, and H_2Te; the absorption coefficient $\alpha = [\log (I_0/I)]/p(\text{atm})/(\text{cm})$. From Rollefson and Burton,[54b] p. 179; originally from Goodeve and Stein.

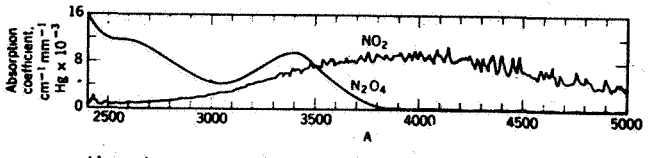

Absorption spectrum of nitrogen dioxide, NO_2, and dinitrogen tetroxide, N_2O_4, at 25° corrected to pure compound spectra. From Hall and Blacet.

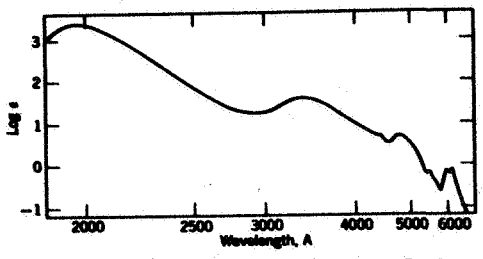

Absorption spectrum of nitrosyl chloride, NOCl. From Goodeve and Katz.

Figure 15. Absorption spectra of selected inorganic molecules.

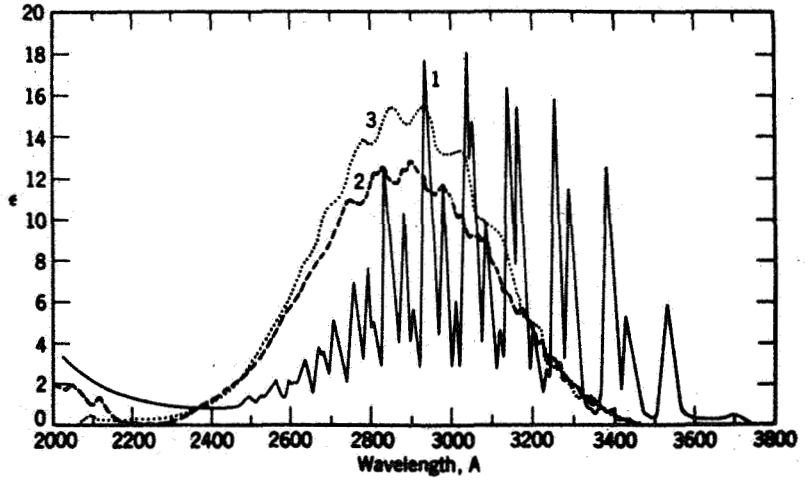

Absorption spectra for (1) formaldehyde [$CH_2O(g)$], ~75°; (2) acetaldehyde [$CH_3CHO(g)$], 25°; (3) propionaldehyde [$C_2H_5CHO(g)$], 25°.

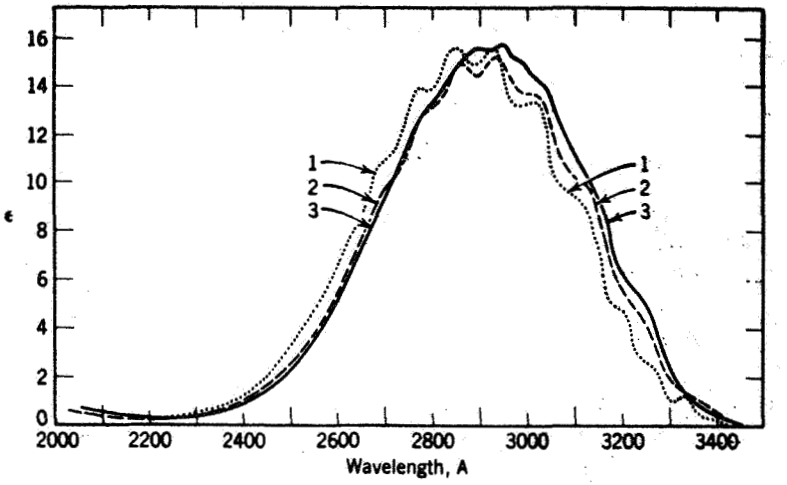

Absorption spectra for (1) propionaldehyde [$C_2H_5CHO(g)$], 25°; (2) *n*-butyraldehyde [n-$C_3H_7CHO(g)$], 25°; (3) isobutyraldehyde [iso-$C_3H_7CHO(g)$], 25°.

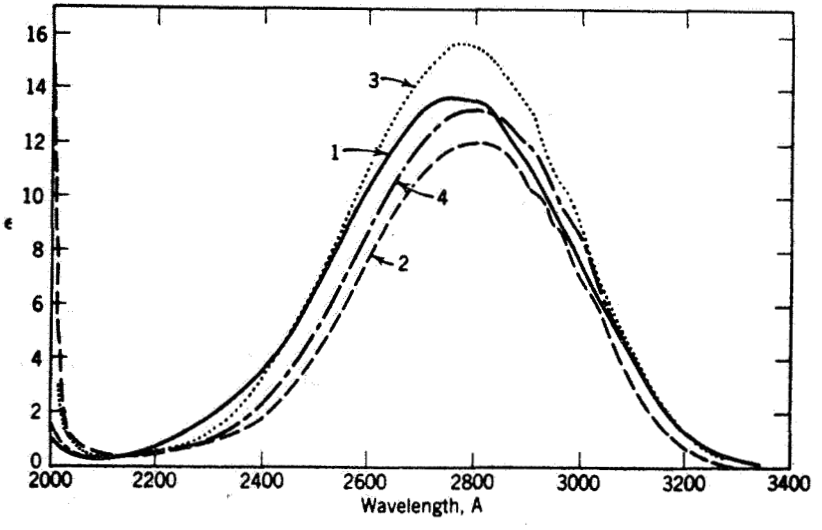

Absorption spectra for (1) acetone [$CH_3COCH_3(g)$], 25°; (2) diethyl ketone [$C_2H_5COC_2H_5(g)$], 25°; (3) methyl ethyl ketone [$CH_3COC_2H_5(g)$], 25°; (4) methyl-*n*-butyl ketone [$CH_3CO(CH_2)_3CH_3(g)$], 25°

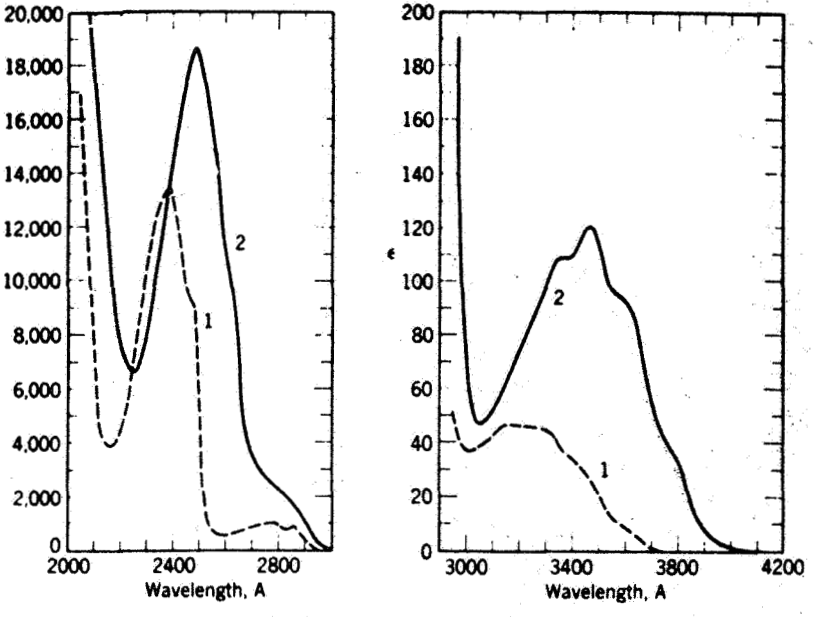

Absorption spectra for (1) acetophenone ($CH_3COC_6H_5$) in cyclohexane, 25°; (2) benzophenone ($C_6H_5COC_6H_5$) in cyclohexane, 25°.

Figure 16. Absorption spectra of selected organic molecules.

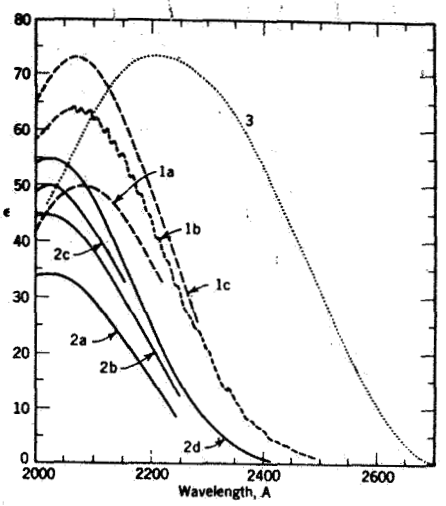

Absorption spectra for (1) formic acid [$CHO_2H(g)$], 27°: (a) 2.45 mm, (b) 16.4 mm, (c) 35.2 mm; undefined amount of monomer and dimer contribute; calculated assuming monomer only; (2) acetic acid [$CH_3CO_2H(g)$], 26°: (a) 3.6 mm, (b) 8.3 mm, (c) 11.0 mm, (d) 12.9 mm; calculated assuming monomer only; (3) acetic anhydride [$(CH_3CO)_2O(g)$], 25°.

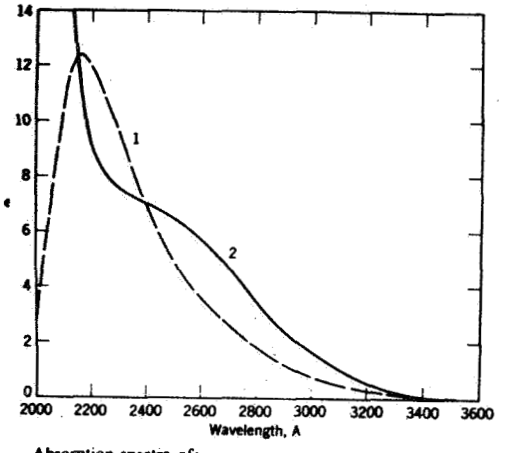

Absorption spectra of:
(1) dimethyl peroxide [$CH_3OOCH_3(g)$], from Takezaki, Miyazaki, and Nakahara;[112a]
(2) di-*tert*-butyl peroxide [$(CH_3)_3COOC(CH_3)_3(g)$], 25°.

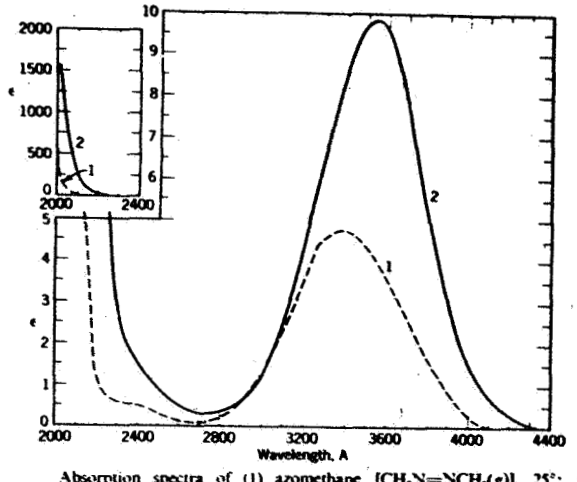

Absorption spectra of (1) azomethane [$CH_3N{=}NCH_3(g)$], 25°; (2) azoethane [$C_2H_5N{=}NC_2H_5(g)$], 25°.

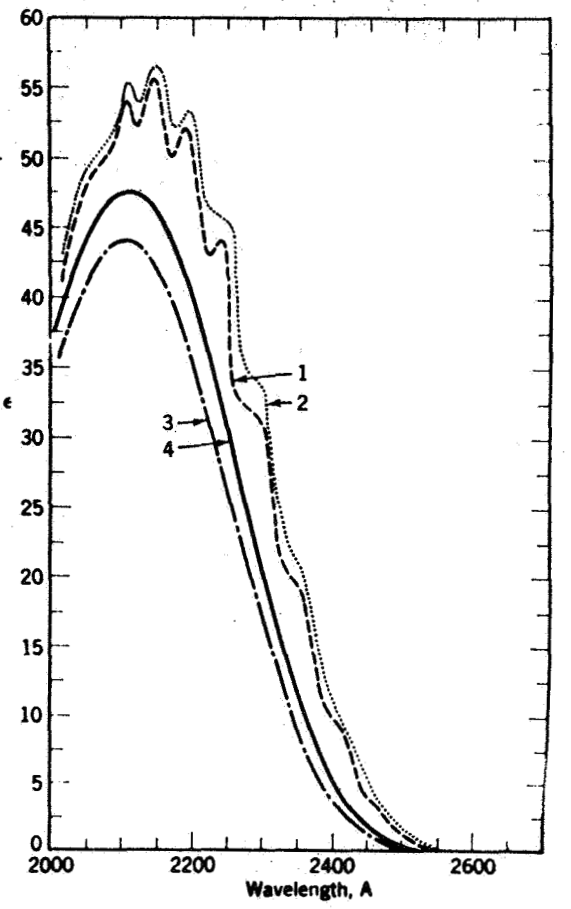

Absorption spectra for:
(1) methyl formate [$CH_3O_2CH(g)$], 25°;
(2) ethyl formate [$C_2H_5O_2CH(g)$], 25°;
(3) methyl acetate [$CH_3O_2CCH_3(g)$], 25°;
(4) ethyl acetate [$C_2H_5O_2CCH_3(g)$], 25°.

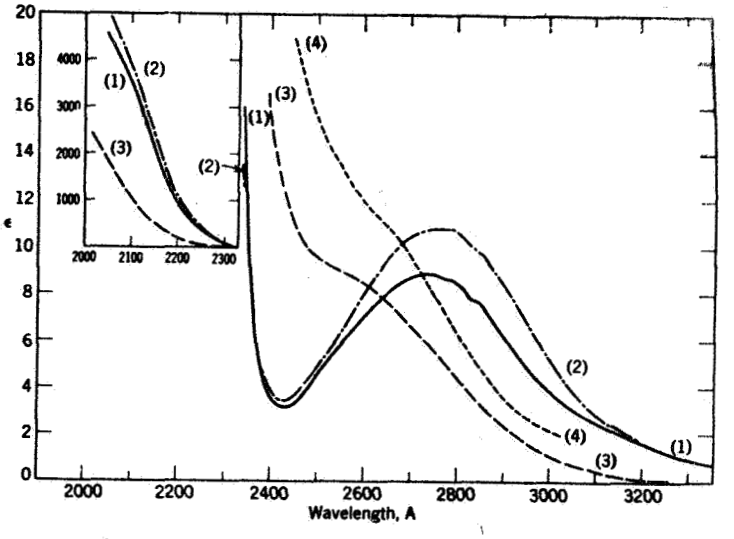

Absorption spectra of (1) nitromethane [$CH_3NO_2(g)$], 25°; (2) nitroethane [$C_2H_5NO_2(g)$], 25°; (3) methyl nitrate [$CH_3ONO_2(g)$], 25°; (4) ethyl nitrate [$C_2H_5ONO_2(g)$], 25°.

Figure 17. Absorption spectra of selected organic molecules.

Absorbing gases (for $\lambda\lambda > 2000\text{Å}$) which may be present in the lower Martian atmosphere may act as photosensitizers to allow solar photolysis of CO_2, HOH, organics, and other molecules which do not absorb the relatively intense solar flux in this spectral region. For example, although CO_2 and water vapor do not absorb strongly in this region, the invocation of of photosensitization by an absorbing species (i.e., SO_2, H_2S) could result in the photolysis of these species and subsequent generation of several simple organic molecules which may have important implications on the exobiology of Mars. In fact, several compounds possibly produced by the above mechanism are also represented in the life-cycle. Characteristically, simple organic compounds often absorb strongly in the region $\lambda\lambda$ 2000-3000Å as illustrated by the data of Figures 16 and 17 pertinent to a variety of formaldehydes, ketones, organic acids, hydrides, and esters. Calvert and Pitts[71] present a number of photolytic mechanisms involving these and other organic materials, the products of which would undoubtedly be important to Martian biological investigations. The detection of these or other organic materials does not intrinsically assure a biological origin, although the presence of these constituents could represent and possibly be identified with key residue materials of biological processes. In this regard, it would be of particular value to review the experimental requirements and expected results of complementary exobiological experiments aboard the Martian Lander.

The salient features of an atmospheric absorption measurement experiment can be discussed both in terms of the geometry illustrated in Figure 7, and the corresponding twilight zenith and horizon radiances presented in Figures 10 and 11, respectively. The detection of minor

constituents will be achieved by performing both zenith and horizon spectral scans ($\lambda\lambda$ 2000-3000Å) throughout twilight observation periods. It can be seen from Figure 7 that a significantly enhanced cm^2 column count is involved along the path ACD. On this basis, the presence of minor constituents along this path would sensitively affect the observed zenith and horizon radiances as a function of both solar depression angle and wavelength. The application of appropriate analytic techniques should result in the extraction of the absorption characteristics of the lower atmosphere and, under certain conditions, specific constituents may be identifiable. Finally, if the major absorption contribution over a given spectral interval can be ascribed to a specific constituent (i.e. NO, CO, OH, CN, etc.), then it might be possible to obtain the scale height or number density-altitude profile for that species. In any event, it is evident that the highly sensitive absorption experiment described above can serve to establish new identifications, upper limit content values and distributions of trace constituents resident in the lower Martian atmosphere.

(5) The Detection and Characterization of Dust in the Martian Atmosphere

There appears to be little question regarding the occasional existence of dust and/or haze layers in the lower Martian atmosphere.[72] Physical, photographic and polarometric measurements have indicated that several cloud forms exist including white,clouds, blue clouds, "yellow veils", and "violet hazes". The white clouds probably involve a particle size range between 1 to 60 microns and are believed to consist of either ice or solid CO_2. It is believed that their formation is favored in low

temperature regions since they have often been observed at the sunrise and sunset limbs of the planet. The blue clouds, characterized probably by a particle size range between 0.1 to 1 micron have been compared by some to terrestrial noctilucent clouds, while others feel they represent an accumulation of micrometeorites suspended in the lower Martian atmosphere. The relatively rarely observed low-level yellow clouds probably consist of white desert dust blown about by Martian surface winds. In summary, it appears that not only is the presence of dust in the Martian atmosphere confirmed, but that the particle diameters appear to range from 0.1 to 60 microns.

The general experimental configuration and the procedures applied herein should closely resemble those described in the previous section concerning detection of trace molecular constituents by absorption differentiation over the spectral region $\lambda\lambda$ 2000-8000Å. However, the conduct of the observations should not be confined to twilight since it certainly appears feasible to search for particulate scattering from dust layers under full solar illuminated daytime conditions as well as during times of Phobos illumination on the night side of the planet.

For the ranges of wavelengths and particle diameters involved, it appears that both Rayleigh and Mie scattering contribute to the observed signals, so that performance of the spectral scanning procedure over the specified geometry should result in confirmation of the presence or absence of dust or haze layers in the lower Martian atmosphere. Additionally, application of appropriate analytic procedures to representative spectral scans under the variety of conditions encountered during the experiment may produce data relevant to the size distribution, nature, and other physical

characteristics of the particulate matter. Twilight observations could be employed for example, to locate the tops of layers. While this latter information is of great interest intrinsically, it could also be applied to the analysis of the other proposed twilight measurement experiments discussed previously.

With respect to nighttime measurements, the white clouds (size distribution from 1 to 60 microns) appear to form in the vicinity of the planetary sunrise and sunset limbs, so that such clouds may exist throughout the entire dark side of the planet owing to the relatively low ambient temperature conditions. This possibility could be verified simply by observing the presence of Mie scattering (far more efficient than Rayleigh scattering) from the particles illuminated by Phobos during its orbit into and around the dark side of the planet. For this particular case, however, preliminary calculations indicate that the relatively low signal intensities involved would probably require that the spectral resolution of the instrument be increased to about 100Å.

Finally, the employment of a polarization disc should be considered in order to acquire pertinent information to further characterize the size, distribution, and physical nature of the observed particles. However, it should be noted that employment of such a polarization disc generally involves signal intensity losses as well as imposing a short wavelength limitation on the observations.

d. Instrumentation

The discussions presented in the previous sections have identified the general operational requirements and constraints of the proposed

instrumentation system. Among the specific requirements are included: (a) spectral scanning capability to cover both the ultraviolet and visible regions from $\lambda\lambda$ 2000-8000Å; (b) a spectral resolution of approximately 1Å would be desirable; (c) a highly ruggedized instrument having minimum moving parts due to the nature of the mission; (d) sensitivity such that brightness values of between 1 to 10 R/Å can be observed over the ultraviolet spectral region; and finally (e) employment of a double-pass configuration in order to minimize significant instrumental scatter problems which may be encountered in the adopted experimental mode.

In this regard, under Contract NAS5-9472 the GCA Technology Division designed a double-pass UV scanning spectrometer for operation in a satellite environment for the purpose of measuring the content and distribution of ozone in the earth atmosphere. The salient features of this latter instrument shown schematically in Figure 18 can be applied directly to the proposed experimental requirements enumerated above. The general features and pertinent operational aspects of the instrument are described elsewhere.[48]

Order of magnitude calculations indicate that the employment of a 5 x 5-cm grating with 2400 lines/mm and a 50-cm focal length would result in the achievement of a 1Å resolution with a slit-width of about 25 microns (if the grating is set for an angle of incidence of 45 degrees as shown in the figure). These calculations also indicate that the resultant photon flux at the exit slit will be about 100 photons/second for an emission rate of ten R/Å. Using these parameters, further analysis indicates that the

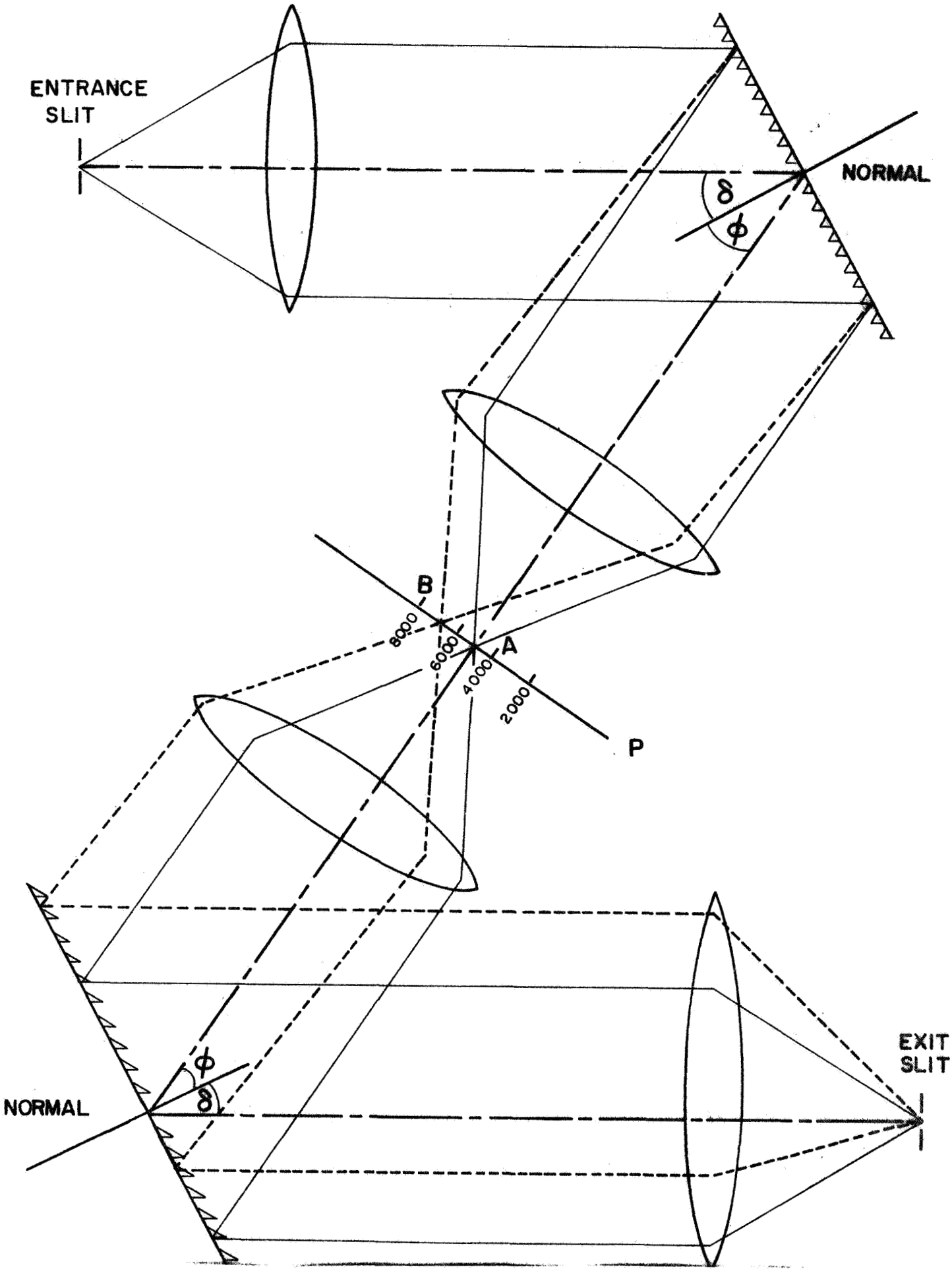

Figure 18. Schematic diagram of proposed instrument.

entire spectral interval from 2000-8000Å would be spread over a length of about 15 cm across the focal plane as shown in Figure 18.

It should be noted that the optical components shown in Figure 18 are schematically indicated by lenses; however, in practice mirrors would be involved. There is no requirement for the optical components to vary their positions during scanning operations so that the fabrication of a ruggedized version of this design should constitute a relatively straightforward task.

Much of the material generated under this study has been utilized in the preparation of a suggested experiment for the forthcoming Mars Lander Program.

III. MISCELLANEOUS

This section contains brief summaries of the scientific material generated under the present program and presented at scientific and/or professional meetings. In addition, there is included other miscellaneous topics of interest in the performance of the current contract committments.

During the current reporting period Dr. James A. R. Samson attended the 21st Annual Gaseous Electronic Conference held at the University of Boulder, Boulder, Colorado, 16-18 October 1968. Dr. Samson presented a paper entitled "Higher Ionization Potentials of Molecules Determined by Photoelectron Spectroscopy". This paper was received with considerable interest since there is an accelerating activity in the new field of electron spectroscopy. Historically, this conference deals with photon-atom interaction, atom-atom interactions, ion-molecule reactions and electron-molecule interactions. Many of these areas are of direct interest to the performance of the current contract committments. Of particular interest to some current problems in photoelectron spectroscopy was a paper entitled "Configuration Mixing of Continuum States" presented by A. J. Mendez. This theoretical paper has been of significant importance in defining future pertinent experimental measurements. For example, it was pointed out that it would be of significant importance to measure the coefficients A and B for the angular distribution of photoelectrons in wavelength regions wherein auto-ionization and overlapping continuum states occur. With the experimental values available, the theoretician could then determine the proper wave functions of the states involved.

During the conference local visits were made to NCAR and ESSA.

E. Ferguson (ESSA) demonstrated laboratory evidence for the reaction $He^+ + N_2 \rightarrow N_2^+ + h\nu$ ($\approx$ 2000Å). This was of special interest to our laboratory effort, since GCA has previously observed "fluorescence" in He at wavelengths shorter than those corresponding to the ionization potential. On the basis of Ferguson's data it would appear then that these emissions could have been due to N_2 impurities in the gas sample.

IV. QUARTERLY PROGRESS REPORT FOR HOURS WORKED IN THE PERIOD 1 SEPTEMBER 1968 THROUGH 30 NOVEMBER 1968.

In compliance with the requirements of the subject contract, the following is an integrated tabulation of total hours worked by labor category and grade.

Labor Category	Labor Grade	Total Hours
*Junior Technician	2	182
*Technician Experimental Machinist	3	178
*Senior Technician Senior Experimental Machinist	4	332
*Junior Scientist Junior Engineer	5	0
*Scientist Engineer	6	60
Senior Scientist Senior Engineer	7	641
Staff Scientist	8	124
Principal Scientist	9	73
Group Scientist	10	1,240

*and other equivalent categories

Quarterly Total..... 2,830

REFERENCES

1. Warneck, P., J. Geophys. Res. 72, 1651 (1967)

2. Warneck, P., J. Chem. Phys. 46, 502 (1967)

3. Saporoschenko, M., Phys. Rev. 111, 1550 (1958)

4. Varney, R. N., Phys. Rev. 89, 708 (1953)

5. Kovar, F. R., Beaty, E. C. and Varney, R. N., Phys. Rev. 107, 1490 (1957)

6. Saporoschenko, M., Phys. Rev. 139, A 352 (1965)

7. Asundi, R. K., Schulz, G. J., and Chantry, P. J., J. Chem. Phys. 47, 1584 (1967)

8. Varney, R. N., J. Geophys. Res. 72, 5578 (1967)

9. Keller, G. C., Martin, D. W. and McDaniel, E. W., Phys. Rev. 140, A 1535 (1965)

10. Curran, R. K., J. Chem. Phys. 38, 2974 (1963)

11. Fite, W. L., Rutherford, A., Snow, W. R. and van Lint, V. A. T., Discussions Faraday Soc. 33, 264 (1962)

12. Rabinovitch, K., Ganfield, L. R. and Madden, R. P., Appl. Optics 4, 1005 (1965).

13. Hamm, R. N., MacRae, R. A. and Arakawa, E. T., J. Opt. Soc. Am. 55, 1460 (1965)

14. Samson, J. A. R., Techniques of Vacuum Ultraviolet Spectroscopy, John Wiley and Sons, New York (1967).

15. Bhagavantam, S. in Scattering of Light and the Raman Effect, Chemical Publishing Company, Inc., New York (1942).

16. Samson, J. A. R., Phys. Rev. 173, 80 (1968).

17. Tanaka, Y., Sc. Papers I.P.C.R., 39, 456 (1942)

18. Dressler, K. and Miescher, E., Astrophys. J. 141, 1266 (1965)

19. Al-Joboury, M. I. and Turner, D. W., J. Chem. Soc. 4434 (1964)

20. Turner, D. W. and May, D. P., J. Chem. Phys. 45, 471 (1966)

21. Price, W. C., Private communication

22. Huber, K. P., Can. J. Phys. 46, 1691 (1968).

23. Salle, M. and Vodar, B., Compt. Rend. 230, 380 (1950) and described in detail in J. A. R. Samson, "Techniques of Vacuum Ultraviolet Spectroscopy" (John Wiley and Sons, New York, 1967).

24. Victor, G. A., Browne, J. C. and Dalgarno, A., Proc. Phys. Soc. (London) 92, 42 (1967).

25. Dalgarno, A. and Davison, W. D., Adv. Atom. Mol. Phys. 2, 1 (1966).

26. Dalgarno, A., Degges, T. and Williams, D. A., Proc. Phys. Soc. (London) 92, 291 (1967).

27. Lassettre, E. N. and Johnes, E. A., J. Chem. Phys. 40, 1222 (1964).

28. Geiger, J., Zeit, Physik, 181, 413 (1964).

29. Geiger, J. and Topschowsky, N., Z. Naturforsch. 21a, 626 (1966).

30. Hesser, J. E., J. Chem. Phys. 48, 2518 (1968).

31. Kock, J., Arkiv. Math. Astron. Fysik. 8, 20 (1912).

Kirn, M., Ann. Physik, 64, 566 (1921).

32. Bridge, N. J. and Buckingham, A. D., J. Chem. Phys. 40, 2733 (1964) Proc. Roy. Soc. (London), A295, 334 (1966).

33. Dieke, G. H., J. of Mol. Spec. 2, 494 (1958).

34. Browne, J. C., J. Chem. Phys. 44, 835 (1966).

35. Ehrenson, S. and Phillipson, P. E., J. Chem. Phys. 34, 1224 (1961).

36. Gill, P. and Heddle, D. W. O., J. Opt. Soc. Am. 53, 848 (1963).

37. Dalgarno, A. and Williams, D. A., Mon. Not. Roy. Ast. Soc. 124, 313 (1962).

38. Schuler, H. and Wolf, K. L., Z. Physik, 34, 343 (1925).

39. Ingersol, L. R., and Liebenberg, D. H., J. Opt. Soc. Am. 46, 538 (1956).

40. Kolos, W. and Wolniewicz, L., J. Chem. Phys. 41, 3674 (1964); J. Chem. Phys. 41, 3663 (1964); J. Chem. Phys. 46, 1426 (1967).

41. Dalgarno, A. and Stewart, A. L., Proc. Phys. Soc. (London) 76, 49 (1960).

42. Bethe, H. A., Ann. Physik, 5, 325 (1930).

43. Dalgarno, A. and Williams, D. A., Proc. Phys. Soc. (London), 85, 685 (1965)

44. Garcia, J. D., Phys. Rev. 147, 66 (1966).

45. Hirschfelder, J. O., Curtiss, C. F. and Bird, R. B., Molecular Theory of Gases and Liquids, (Wiley, New York, 1954).

46. Casimir, H. B. G. and Polder, D., Phys. Rev. 73, 360 (1948).

47. U. S. Standard Atmosphere Supplements, 1966

48. Marmo, F. F., GCA Final Report NASW-1283 (July, 1968)

49. Schultz, E. D. and Holland, A. C., GCA TR 62-14-N (November, 1962)

50. Sullivan, J. O. and Holland, A. C., GCA TR 64-16-A (December, 1964)

51. Marmo, F. F., Quarterly Progress Report No. 1, NASW-1726, (August, 1968)

52. Chamberlain, J. W., Physics of the Aurora and Airglow, Academic Press, New York (1961)

53. Noxon, J. F. and Goody, R. M., Journal of Atmospheric Science, 19, 342 (1963)

54. Donahue, T. M., et al, Journal of Geophys. Res. 72, No. 11, 2803 (1967).

55. Narcisi, R. S., Cospar, Space Research VIII, Editors, Mitra, A. P., Jacchia, L. G. and Newmann, W. S., North Holland Publishing Co., Amsterdam (1967).

56. Vallance Jones, A., Planetary and Space Science, 10, 117 (1963).

57. Marmo, F. F. and Brown, H. K., GCA TR 63-4-N (March, 1963)

58. Aller, L. H., The Abundance of the Elements, Vol. VII, pps. 54-55 and 122-123, Interscience Publishers, Inc., New York (1961)

59. Allen, C. W., Astrophyskcal Quantities, Second Edition, Athlane Press, London (1963).

60. Marmo, F. F., et als, GCA TR 65-13-N (June, 1965)

61. Chamberlain, J. W. and Sobouti, Y., Astrophysical Journal, 135, 925 (1962)

62. Chandrasekhar, S., Radiative Transfer, Dover Publications, New York (1960)

63. Barth, C. A. U V Spectroscopy of Planets, JPL TR No. 32-822 (December 15, 1965)

64. Inn, E. C., Journal of Atmospheric Sciences, 21, 220 (1964).

65. Mahan, B. H. and Solo, R. B., Journal of Chemical Physics, 37, No. 11, 2669 (1962).

66. Clyne, M. A. A. and Thrush, B. A., Proc. Roy. Soc. 269A, 404 (1962).

67. Marmo, F. F. and Warneck, P., Quarterly Progress Report No. 4, NASW-840 (October 15, 1964)

68. Belton, M. J. S. and Hunten, D. M., The Astrophysical Journal, 153, 963 (1968)

69. Jonathan, N., and Doherty, G., GCA TR 63-1-N (February, 1963)

70. Evans, D. C., Science, 149, 969 (1965)

71. Calvert, J. G. and Pitts, J. N. Jr., Photochemistry, Wiley and Sons, Inc., New York (c.1966)

72. Cadle, R. D., Particles in the Atmosphere and Space, Rienhold Publishing Corporation, New York (1966).